5-17-2014

Fiber Loop Ringdown Gas Flow and Humidity Sensors

Haifa Hassan Alali

Fiber loop ringdown gas flow and humidity sensors

By

Haifa Hassan Alali

A Thesis
Submitted to the Faculty of
Mississippi State University
in Partial Fulfillment of the Requirements
for the Degree of Master of Science
in Physics
in the Department of Physics and Astronomy

Mississippi State, Mississippi

May 2014

Fiber loop ringdown gas flow and humidity sensors

By

Haifa Hassan Alali

Approved:

_____

Chuji Wang
(Major Professor)

_____

David L. Monts
(Committee Member/Graduate Coordinator)

_____

Hendrik F. Arnoldus
(Committee Member)

_____

R. Gregory Dunaway
Professor and Dean
College of Arts & Sciences

Name: Haifa Hassan Alali

Date of Degree: May 17, 2014

Institution: Mississippi State University

Major Field: Physics

Major Professor: Chuji Wang

Title of Study: Fiber loop ringdown gas flow and humidity sensors

Pages in Study: 92

Candidate for Degree of Master of Science

Fiber optics has been utilized in fiber optic, sensing technology, imaging optics, communications, etc. Fiber optic sensors have been developed to sense in many applications. In this thesis, fiber loop ringdown (FLRD) sensors were used to monitor two different physical sensors, such as gas flow and humidity.

FLRD gas flow sensors were demonstrated. Two different sensor configurations were constructed to monitor airflow (AF). FLRD-AF sensor was based on micro-bending mechanism. The FLRD-AF sensor was able to detect AF in a range of 5 to 22.5 slpm.

FLRD technique was also used to measure relative humidity (RH). A sensor was fabricated and replaced inside a chamber. The chamber provided with humidity reference and a humidity meter. The FLRD-RH was based on evanescent field mechanism. The RH and the temperature were monitored during the experiment. The FLRD-RH has a dynamic range of 4 to 100 %.

DEDICATION

To my King Abdullah bin Abdulaziz Al Saud

Who gave me this opportunity to continue my education and supported me financially.

To my wonderful and lovely mother

Who encouraged me and inspired me at every step of my life.

Without her support, I would not reach to this goal.

To my great and loving father

Who supported me and encouraged me throughout my life.

I am a lucky girl to have parents like them.

To my lovely, wonderful and lucky fiancé (Mohammed)

for his support and encouragement.

ACKNOWLEDGEMENTS

I would like to express the deepest appreciation to my research advisor, Dr. Chuji Wang, whose encouragement, guide, teaching, and support me to achieve this goal. His enthusiasm, eternal energy, and wisdom in research have motivated all his advisees, including me. This thesis would not have been finalized without his guidance.

In addition to my advisor, I would like to thank the rest of my committee members: Dr. David L. Monts and Dr. Hendrik F. Arnoldus for their time and support.

I would like to express my heartfelt thanks to my lab mates and all the members in our research group: Dr. Malik Kaya, Dr. Peeyush Sahay, Wei Wu, Zhenan Wang, Mahesh Ghimire, Che Fuh, Diana Hubis, and Jonathan Miller for their assistance, support, and for the fun we had. I would like to thank Susan Galloway, Ben Ardahl, Robertsen Riehle, and Brad Bennett for help and assistance.

I am very thankful to my mother, father, brothers: Abdulaziz, Hisham, Mohammed, and Fawaz, sisters: Nihad and Hebah, fiancé, families, and friends for supporting and encouraging me through my study. Special thanks to my lovely fiancé (Mohammed) for his support and encouragement.

This work was supported by the National Science Foundation (NSF) through the grant CMMI-0927539.

TABLE OF CONTENTS

LIST OF TABLES

LIST OF FIGURES

ABBREVIATIONS

FLRD: fiber loop ringdown

FOS: fiber optic sensor

CRDS: cavity ringdown spectroscopy

TIR: total internal reflection

RI: refractive index

MMF: multi-mode fiber

HF: hydrofluoric

SMF: single mode fiber

SH: sensor head

AF: airflow

Slpm: standard liter per minute

FLRD-AF: fiber loop ringdown- airflow

RH: relative humidity

FBG: fiber Bragg grating

LPG: long period grating

DI: deionized

CW: continuous wave

EF: evanescent field

EF-FLRD: evanescent field- fiber loop ringdown

TFBG: tilted fiber Bragg grating

POF: plastic optical fiber

HFG: hybrid fiber grating

PCF: photonic crystal fiber

RPC: resistive plate counters

ppm: parts per million

D/F PT: dew/frost point

N: nitrogen gas

LSPR: localized surface plasmon resonance

LMR: lossy-mode resonance

CHAPTER I

INTRODUCTION

An optical fiber is transparent fiber and is made of plastic or glass (silica). The optical fiber transports light as a waveguide [1]. Thus, an optical fiber is mainly utilized in telecommunication because optical fiber cables can transmit data over long distances with low loss. Over the last 40 years, fiber optic sensors have applied to several applications for sensing, such as chemical, physical, and biomedical [2,3]. In this thesis, the main focus is on physical application, such as detecting gas flow and monitoring relative humidity using the fiber loop ringdown (FLRD) technique. Chapter I describes fiber optic sensors (FOS) and their advantages, cavity ringdown spectroscopy (CRDS), the FLRD technique and its advantages, the FLRD principle, and FLRD system instrumentation.

1.1 Fiber Optic Sensors

Basically, a fiber optic sensor (FOS) system includes a section of optical fiber, a light source (e.g., laser source), a photodetector, and electronic devices that could include a current controller, a pulse generator, an oscilloscope, a temperature controller, and a computer. The fundamental principle of optical fiber light transfer is based on total internal reflection (TIR) principle [4]. Light travels through the fiber core because of the TIR phenomenon. The optical fiber contains of fiber cladding that has a large refractive

index (RI) and a fiber core, which has a smaller refractive index. The cladding RI has to be larger than the core RI because light propagation in the fiber core follows the TIR principle. When the light falls on the boundary of any two media that have two different RI and the incident angle is equal or larger than the critical angle, the light will remain to the TIR principle, which can be illustrated by Snell's law as [5].

$$\theta_c = sin^{-1}\left(\frac{n_2}{n_1}\right) \tag{1.1}$$

When a sensing event needs to be sensed, the FOS principle measures a light frequency shift or electromagnetic energy, which is known as the intensity-domain technique. The term coined today is frequency-domain technique. There are two different utilities for FOS, such as extrinsic sensors and intrinsic sensors. In extrinsic FOS sensors, the fiber cables, originally a multi-mode fiber (MMF) is used to transfer the procedure light from a sensor to the transmitter. An extrinsic sensor has the capability to get unreachable places (e.g., aircraft jet engines) to monitor temperature [6]. Moreover, extrinsic sensors are excellent at producing lower noise when monitoring signals. More details about extrinsic sensor principles can be seen in [7]. FOSs have been applied to sense several quantities, including physical, chemical, and biological. The optical fiber sensors can be categorized based on the application as biomedical sensors (e.g., glucose content, detect bacteria, etc.) [17,18], chemical sensors (e.g., detect different elements, gas concentration, liquid concentration, etc.) [19,20], and physical sensors (e.g., gas flow, humidity, pressure, temperature, crack, etc.) [21-24].

1.1.1 Advantages of Fiber Optic Sensors

Sensors based on fiber optics have many advantages that make them unique compared to other sensors. The FOSs are obtainable in small sizes and lightweight. There is no electrical disturbance to other instruments due to their immunity to electromagnetic interference. Because they contain electrically insulating materials, they can be employed in high voltage settings. Moreover, they are safely used in flammable or explosive settings because there is no risk of electric sparks. Also, they do not need electrical cables. Since their materials are chemically passive, there is no chance of corrosion or contamination in the surrounding area. In addition, multiple sensors can be integrated in a single fiber line via a single optical source. They have the capability to operate over a wider range of temperature (i.e., – 60 °C to 85 °C), which no other electronic devices can do. They have the ability to be configured to any shape. Even with high bandwidth, optical fiber sensors have the capacity to transfer high data amounts. It is also possible to setup a sensor network. Optical fiber sensors are highly sensitive and low cost. More explanations about FOS can be seen elsewhere [25-27].

Even though the FOSs have several advantages that make them unique to utilize, FOSs have to be wrapped with protective materials or chemically covered because of their fragility. Also, some work with FOS needs extra caution. Some work with FOS needs to use some expensive equipment, including receivers or transmitters [28].

1.2 Fiber Loop Ringdown Spectroscopy

1.2.1 Origin of Fiber Loop Ringdown Spectroscopy

During the last several years, fiber loop ringdown (FLRD) spectroscopy has been introduced for several sensing applications. The fundamental idea of FLRD involves

from the well-known cavity ringdown spectroscopy (CRDS) [29-31]. CRDS is a highly sensitive technique, which is obtained from the multi-pass nature of an optical absorption path. A schematic of the CRDS concept is illustrated in Figure 1.1. The typical instrumentation of the CRDS technique consists of a laser souse, an oscilloscope, two highly reflective mirrors (≥ 99%), and a photodiode detector. In CRDS, a small fraction of a laser pulse is sent into the first mirror and transferred into the cavity. The cavity length is the distance between the faces of two highly reflective mirrors. A small fraction of the light travels back and forth between the two mirrors inside the cavity. Exponential decay of the light intensity results from loss of the light intensity through each mirror during each pass of the light. A photodiode detector captures the small portion of the light that is transmitted through the second mirror. The waveform of the ringdown decay is shown on an oscilloscope. The exponential decay and ringdown time, "the decay constant", shown from the light intensity inside the cavity is given by

$$\tau = \frac{d}{c|\ln R|} \tag{1.2}$$

where d, c, and R are the cavity length, the speed of the light in a vacuum, and the reflectivity of the mirrors (high reflective mirrors R≈1)

$$\tau = \frac{d}{c(1-R)} \tag{1.3}$$

Since CRDS has been utilized for weak absorption measurements, CRDS has been developed for sensing and trace gas analysis [32].

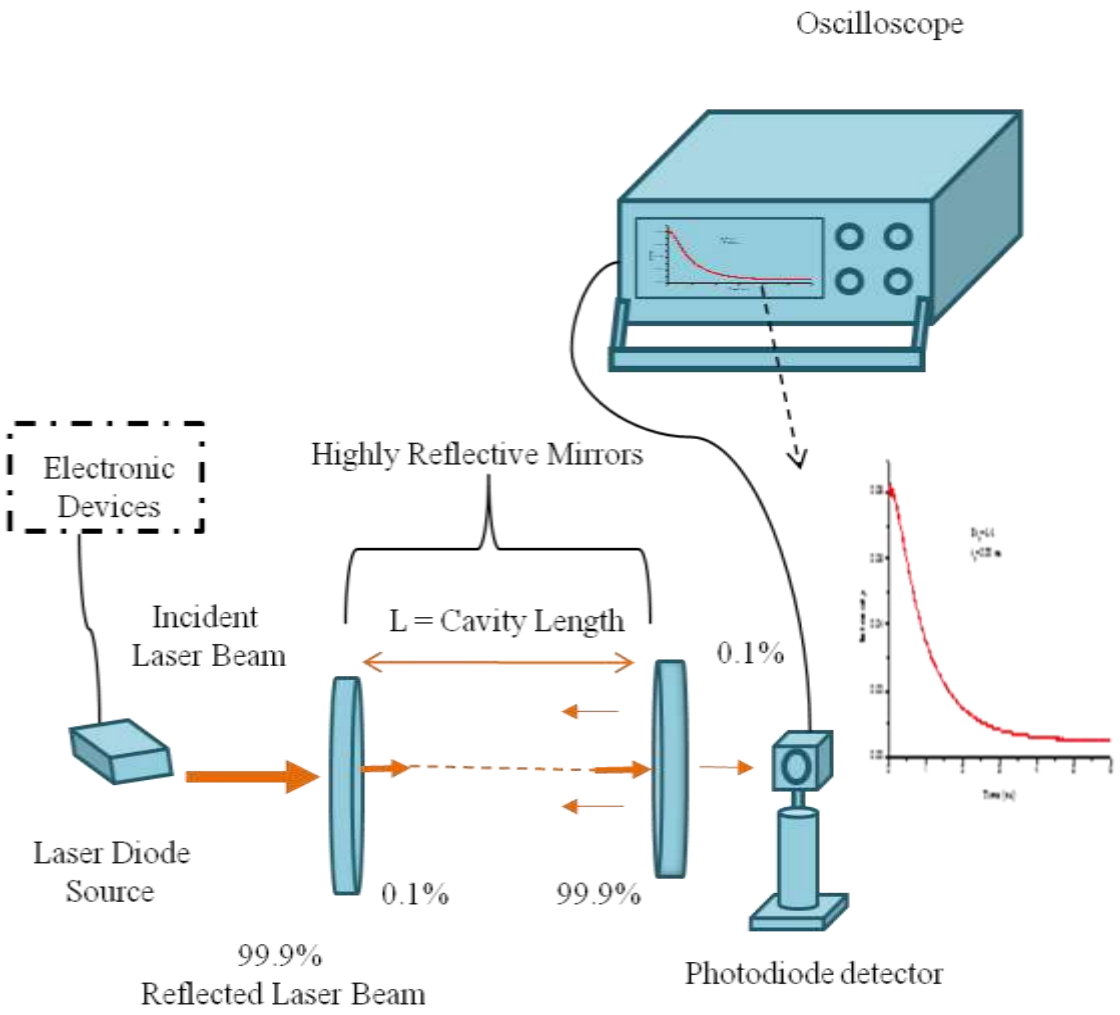

Figure 1.1 Schematic concept of CRDS technique

Incident laser beam from the first high reflective mirror and transmitted laser beam from the second high reflective mirror is monitored via the photodiode detector and the signal is transferred to the oscilloscope to detect the ringdown curve.

1.2.2 Fiber Loop Ringdown Technique

The FLRD technique is originally from the CRDS technique that has been utilized to develop and fabricate FOS sensors based on the time-domain sensing technique [29,33-34]. The differences between the FLRD system and the CRDS system are shown in the construction of the system. In FLRD, the length of the fiber loop is typically 120

m, which is considered the length of the cavity. Also, there are two couplers in the fiber loop similar the high reflective mirrors, as is presented in Figure 1.2.

The FLRD sensing system consists of two main parts: a sensor unit and a control unit, including a photodiode detector, a laser source, and electronic devices for system control and data collection [29]. The sensor unit contains a fiber loop with typically 120 m length, a sensing output (sensor head), and couplers FC/APC fiber connectors for connecting and disconnecting. The coupler has ratio of 0.1/99.9 in a single mode fiber (SMF) coupler. A typical schematic of the FLRD technique is shown in Figure 1.2.

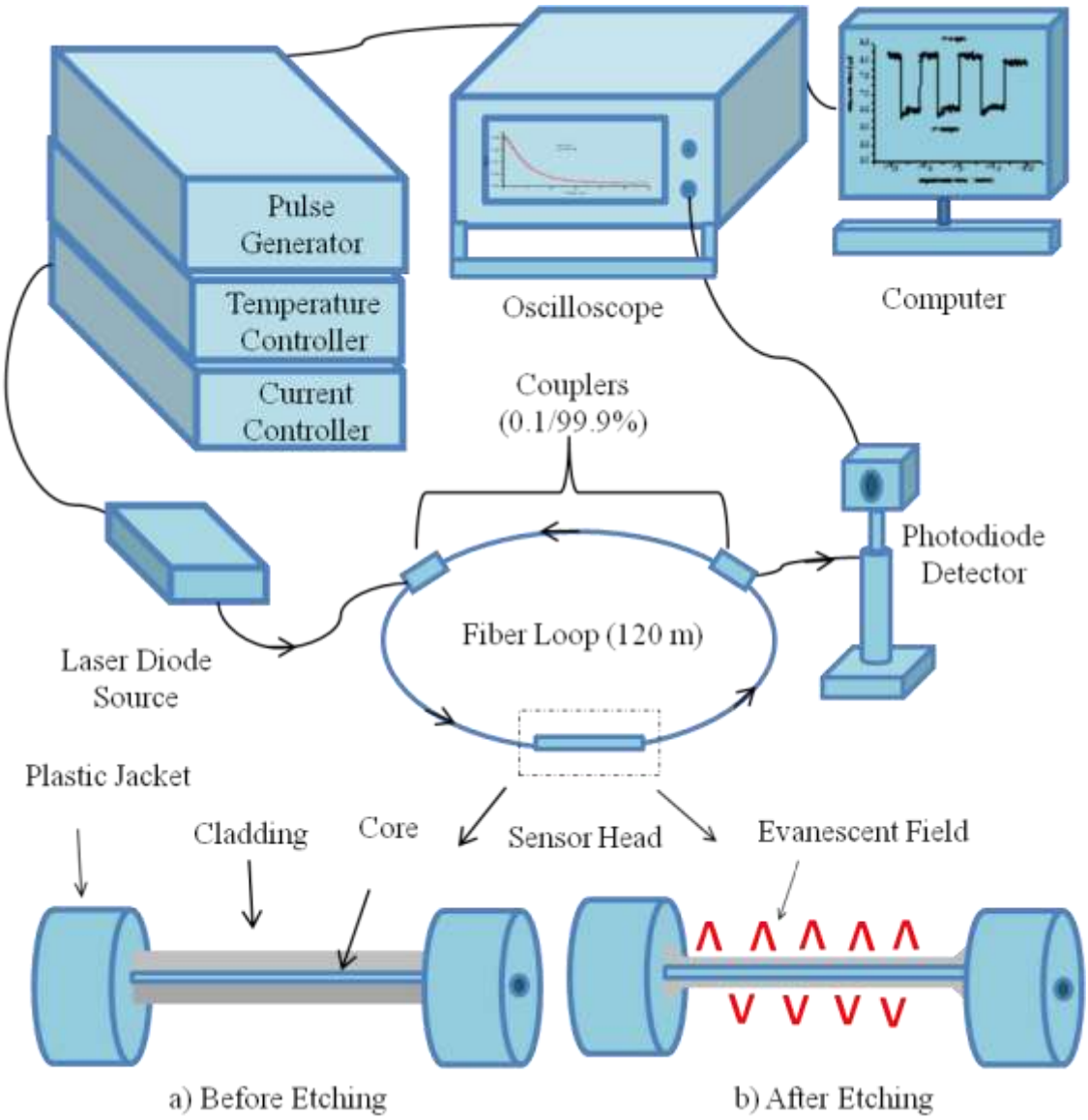

Figure 1.2 Schematic explanation of FLRD sensing technique

The light beam is transferred through the second coupler and collected via a photodiode detector and the signal is transferred to oscilloscope to detect the ringdown curve. (a). It shows the sensor head before etching with 48% HF solution. (b). It shows the sensor head after etching with 48% HF solution. The evanescent field is shown in the surrounding surface of the sensor head by a small spike, which occurs on the surface of the sensor head that intersperses from the core to the external medium.

After the light pulse from the laser source is injected into the fiber loop, the light pulse travels inside the fiber loop for many round trips [29]. A small part of the light

pulse leaks out from the fiber loop to the photodetector through a fiber coupler after each round trip. The remainder of the light keeps traveling in the fiber loop, experiencing fiber transmission losses. The photodetector observes the output signal, which follows an exponential decay. The photodetector transmits the output signal to an oscilloscope, and the oscilloscope shows a ringdown decay waveform. Figure 1.3 illustrates the decay behavior of the light intensity, which is observed by the photodetector. Each of the discrete spikes demonstrates the intensity of the light leaking out of the fiber loop after each around trip. The time between two adjacent spikes represents the time of a light round trip inside the fiber loop. The photodiode detector observes the signal as a series of spikes that represent the envelope decaying exponentially over time. A longer ringdown time (a slower decay rate) is associated with a lower optical loss of light in the fiber loop.

The sensor head (SH) was fabricated in our lab. After removing the plastic jacket from a small section of single mode fiber (SMF), the SMF section was fully immersed in a 48% hydrofluoric (HF) acid solution for 33-34 min for etching processes. Different sensor heads can be constructed for different sensing quantities, as shown in Figure 1.4. More detail about the etching procedure can be seen elsewhere [35].

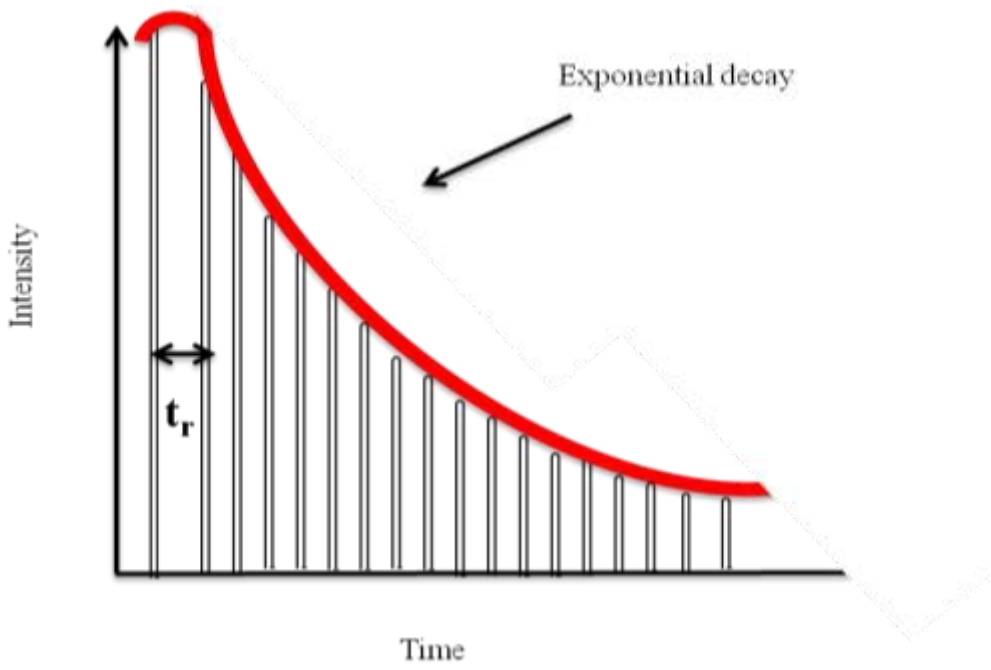

Figure 1.3 FLRD measures the decay rates for determining a quantity.

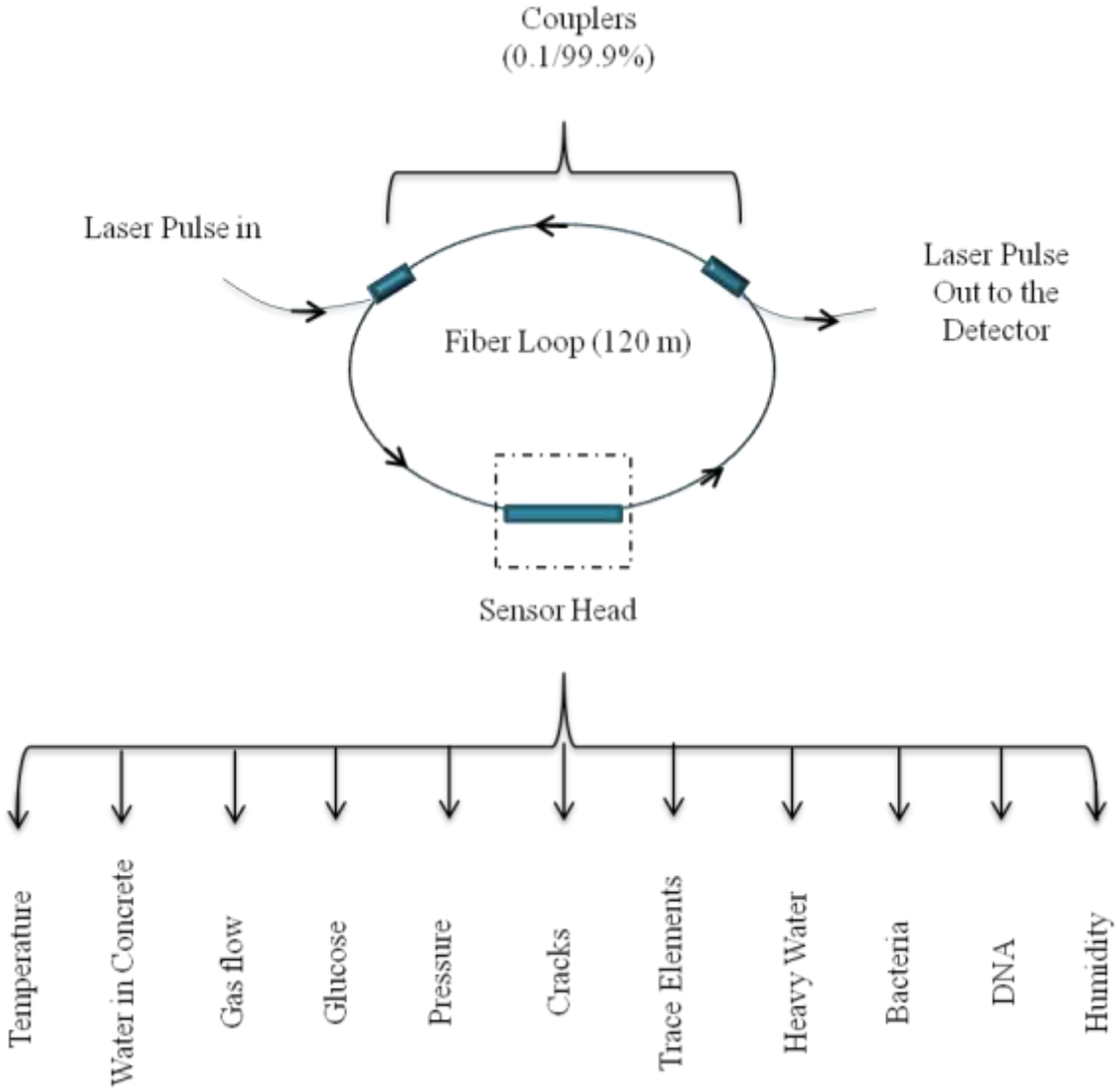

Figure 1.4 Different FLRD sensor heads for detecting different parameters

1.2.3 Advantages of the FLRD Technique

Over the past several years, the FLRD technique has been widely employed to sense many physical quantities, such as temperature [36], pressure [37], cracks [38], water in concert [39], etc. The FLRD technique has several advantages such as [30]:

- Time-domain sensing technique

- Fast response (μs), depending on fiber length and optical losses
- High sensitivity
- Near-real time monitoring because of the multi-pass feature of light pulse inside the fiber loop
- Insensitivity to intensity fluctuations of the laser source
- Low laser power (~μW)
- Multiple sensor units can be allowed
- No need for optical amplification
- No amplified spontaneous emission (ASE) noise needed
- The ability to configure the FLRD sensor head to different sensing quantities (e.g., from fiber Bragg grating for measuring temperature to an air-gap for chemical sensing) without changing any settings
- Low cost
- Large-scale multi function sensor network improvement

1.2.4 Principle of Fiber Loop Ringdown

A light pulse is injected into a fiber loop and travels (rings) inside the fiber loop for many trips. During each round trip, a small portion of the light leaks out of the loop into a photodiode detector through a fiber coupler. The rest of the light remains traveling inside the fiber loop, experiencing inner fiber transmission losses. The photodiode detector observes the output signal, which follows an exponential decay. This behavior can be expressed as [29,30]

$$\frac{dI}{dt} = -\frac{IAc}{nL} \tag{1.4}$$

where I is the light intensity at time t (time equals zero when the light source is shut down and a light pulse is injected into the loop), L is the total length of the fiber loop, n is the averaged-refractive index of the fiber loop, c is the speed of the light in a vacuum, and A is the total fiber transmission loss of the light for each round trip (by percentage). The total fiber transmission loss, A, includes the coupling losses, the fiber absorption loss, and the fiber scattering loss, which can be written as

$$A = \alpha L + E + \gamma \tag{1.5}$$

where α is the wavelength-dependent absorption coefficient for the fiber core material with units, i.e., cm $^{-1}$; γ is the total fiber scattering loss; and E is the total coupling loss at the two points (in and out). The solution of Eq. (1.4) explains the temporal behavior of the light "exponential decay", which is observed by the photodiode detector:

$$I = I_0 \, e^{-\frac{c}{nL}At} \tag{1.6}$$

In Equation (1.6), the FLRD technique measures the light intensity decay rate, not absolute intensity changes, ΔI. Thus, the measurement of A is insensitive to instabilities of the incident light intensity I_0.

The required time for the light intensity I to drop to 1/e of the initial light intensity I_0, as observed by the photodiode detector, is indicated to as ringdown time, τ_0, and is given by

$$\tau_0 = \frac{nL}{cA} \tag{1.7}$$

$$t_r = \frac{nL}{c} \tag{1.8}$$

$$\tau = \frac{nL}{c\,(A+B)} \tag{1.9}$$

Where A is the total transmission loss and it is a constant for a given FLRD sensor, such as temperature, pressure, cracks, or strain sensor. The total transmission loss is estimated by the physical parameters of the sensor, including the coupling losses, the fiber absorption loss, the length of the fiber, and the refractive index. Clearly, when the losses of the light in the fiber are lower, the decay time constant (τ_0) will be longer. Any external action, including absorption or a change of any measureable (strain, pressure, temperature, etc.), happens at any part (sensor head) of the fiber loop. Consequently, an additional optical loss, B, of the light pulse in the fiber loop causes a change in the ringdown time (sensing signal) τ_0 to τ is given by Eq. (1.9).

From Equations (1.7), (1.8) and (1.9), we obtain

$$B = \frac{nL}{c}\left(\frac{1}{\tau} - \frac{1}{\tau_0}\right) \tag{1.10}$$

Equation (1.10) describes the FLRD technique principle. A change in a sensing activity (e.g., fiber mechanical deformation, gas absorption, etc.) for a given sensor is defined by measuring the ringdown time with and without the sensing activity. The term $(1/\tau - 1/\tau_0)$ has a linear relationship with activity-induced optical loss B. In the EF-FLRD sensor, B is associated with the evanescent field-induced optical loss. On the other hand, B will be the optical loss because of any FLRD sensing activity, including gas absorption, bending, etc.

For chemical and biological applications, the detection sensitivity of EF-FLRD sensors is described in the same way via the minimum detectible evanescent field-induced optical loss. Otherwise, for physical applications, the detection sensitivity of EF-

FLRD sensors is described via monitoring sensing activities, including mechanical deformation, bending loss, etc. from Equations (1.10) and (1.8)

$$B = \frac{t_r}{t_0}\frac{\Delta\tau}{\tau} = \frac{1}{m}\frac{\Delta\tau}{\tau} \tag{1.11}$$

$$\Delta\tau = \tau_0 - \tau \tag{1.12}$$

where m is the number of the round trips and τ_r is the round trip time of the laser beam in the fiber loop Eq. (1.8). Consequently, the minimum detectable optical loss, B_{min} which is determined as the one standard deviation σ detection limit, is expressed by

$$B_{min} = \frac{1}{m}\frac{\Delta\sigma_\tau}{\tau} \tag{1.13}$$

where σ_t is the 1σ standard deviation of the ringdown time. $\Delta\sigma_t/\tau$ is the amount of the typical minimum detectible change in the light intensity, $\Delta I/I_0$, which can be experimentally defined at the value of $\sim 10^{-3}$ [30].

For any given sensor to detect any quantity, such as pressure, temperature, bacteria, chemical, cracks, etc, optical loss B has to be modified. For example, for pressure sensors, optical loss B in Equation (1.10) can be given as

$$B = \beta l f \tag{1.14}$$

where β is the pressure-induced loss coefficient (e.g., $Pa^{-1}\ m^{-3}$), l is the length of the fiber that is contacted with applied pressure, and f is an external force on the sensor, which is equal to PS where is P is the external pressure (in pascals) and S is the intersection with the sensor head (m^2). Equation (1.15) can be written in terms of Equation (1.10), which gives the ringdown time measurement for a pressure sensor

$$\frac{1}{\tau} = \frac{1}{\tau_0} = Kf \tag{1.15}$$

where K = $c\beta lS/nL$ is a constant. Ringdown time can be calculated from Equations (1.5), (1.14), and (1.15) when an external force is applied to the sensor head. A is much smaller and first order approximation is written as

$$\tau = \tau_0 \left(1 - \frac{\beta l}{\alpha L + E} f\right) \tag{1.16}$$

Equation (1.16) explains the linear relationship between the measured ringdown time and applied force [23,37].

For cracking sensors, a section of SMF (sensor head) was used to detect cracking. A small part of the SMF (sensor head) had a stretch of ΔL, thus a loss of $\alpha \Delta L$ is occurred. Hence, Equation (1.7) can be rewrite as

$$\tau = \frac{n(L + \Delta L)}{c(A + \alpha \Delta L)} \tag{1.17}$$

The stretches can be ignored when the stretches are small (e.g., millimeters). Because the standard fiber loop length is 120 m and the resultant optical loss is very smaller than the total optical loss of the loop. Equation (1.17) can be modified after using the first order approximation as

$$\tau = \tau_0 \left(1 - \frac{\alpha}{A} \Delta L\right) \tag{1.18}$$

Equation (1.18) demonstrates the relationship between the ringdown time measurement and the stretch length [38].

In this thesis, the main target is to monitor gas flow and relative humidity. For gas flow sensors, two different configurations were constructed to detect airflow at different

flow rates. The sensing mechanism is based on micro-bending [38,40]. The relationship between the ringdown time and the airflow rates was investigated. Assume a small micro-bending happens on the surface of the sensor head when the airflow source is turned on. Since the airflow creates micro-bending that occurs in the small part of the etched single mode fiber (sensor head), the total optical loss B can be given as δF , where is F is the flow rate and δ is the loss per unit volumetric flow rate. Consequently, the optical loss B in Equation (1.9) can be modified to measure the ringdown time, τ, for airflow sensing as

$$\tau = \frac{nL}{c(A+ \delta F)} \tag{1.19}$$

From Equation (1.10) and (1.19), the optical loss can be expressed as

$$\left(\frac{1}{\tau} - \frac{1}{\tau_0}\right) = \frac{c}{nL} B = \frac{c\delta F}{nL} = KF \tag{1.20}$$

where $K = c\ \frac{\delta}{nL}$. Equation (1.20) indicates a linear relationship between the flow rate F and $\left(\frac{1}{\tau} - \frac{1}{\tau_0}\right)$, with K as the constant. Chapter II explains more details about FLRD gas flow sensors.

For a relative humidity sensor, an evanescent field-fiber loop ringdown (EF-FLRD) technique was used to monitor different values of relative humidity. The EF-FLRD technique is based on refractive index (RI) measurement, which measures the optical loss in terms of ringdown time. Since each medium has various RIs, the sensor response depends on changes of the medium around the SH, which change the ringdown time [41]. For relative humidity, the presence of different moisture levels in the chamber changes the refractive index of the medium; thus the ringdown time changes due to a change in EF scattering loss induced in the SH. Therefore, the optical loss B in Equation

(1.10) is used to monitor different relative humidity values. More explanation can be read in Chapter III

1.3 FLRD System Instruments

The FLRD system contains a single mode fiber (fused sillica), two 2 × 1 fiber couplers, a continuous wave (cw) diode laser source, an oscilloscope, a photodiode detector, and electronic controls which contain a temperature controller, a current driver, and a pulse generator.

1.3.1 Single Mode Fiber and Fiber Couplers

The total length of the single mode fiber loop (SMF 28, Corning, Inc) was 120 m. The fiber consists of three layers of a plastic jacket, cladding, and core with diameters of ~ 245 μm, 125 μm, and ~ 8.2 μm, respectively. The operating temperature of the SMF is in the range of – 60 to 85 °C. In addition, the SMF has two identical 2 × 1 fiber couplers (Opneti Communications Co., Hong Kong). Figure 1.5 illustrates the structure of the SMF loop, couplers, and sensor head. At the two-leg end, the two identical fiber couplers were fabricated with a split ratio of 0.1:99.9. The couplers were used to transfer 0.1 % out and reflect 99.9 % back at the incoming laser beam. More details about the couplers and SMF can be found in [42,43]. A small section in the middle of the fiber loop (SMF), i.e., 3 – 12 cm, was fabricated to serve as sensor head, followed by etching with 48% hydrofluoric acid (HF) solution. The sensor was connected and disconnected from the control system by two single mode fiber FC/APC connectors. One is connected to the laser source and the other to the photodiode detector. In order to fabricate the sensor

head, several tools need to be used, such as an optical fiber cleaver, fiber splicer (Fusion Splicer, PRO 730), and a stripper [44], as seen in Figure 1.6.

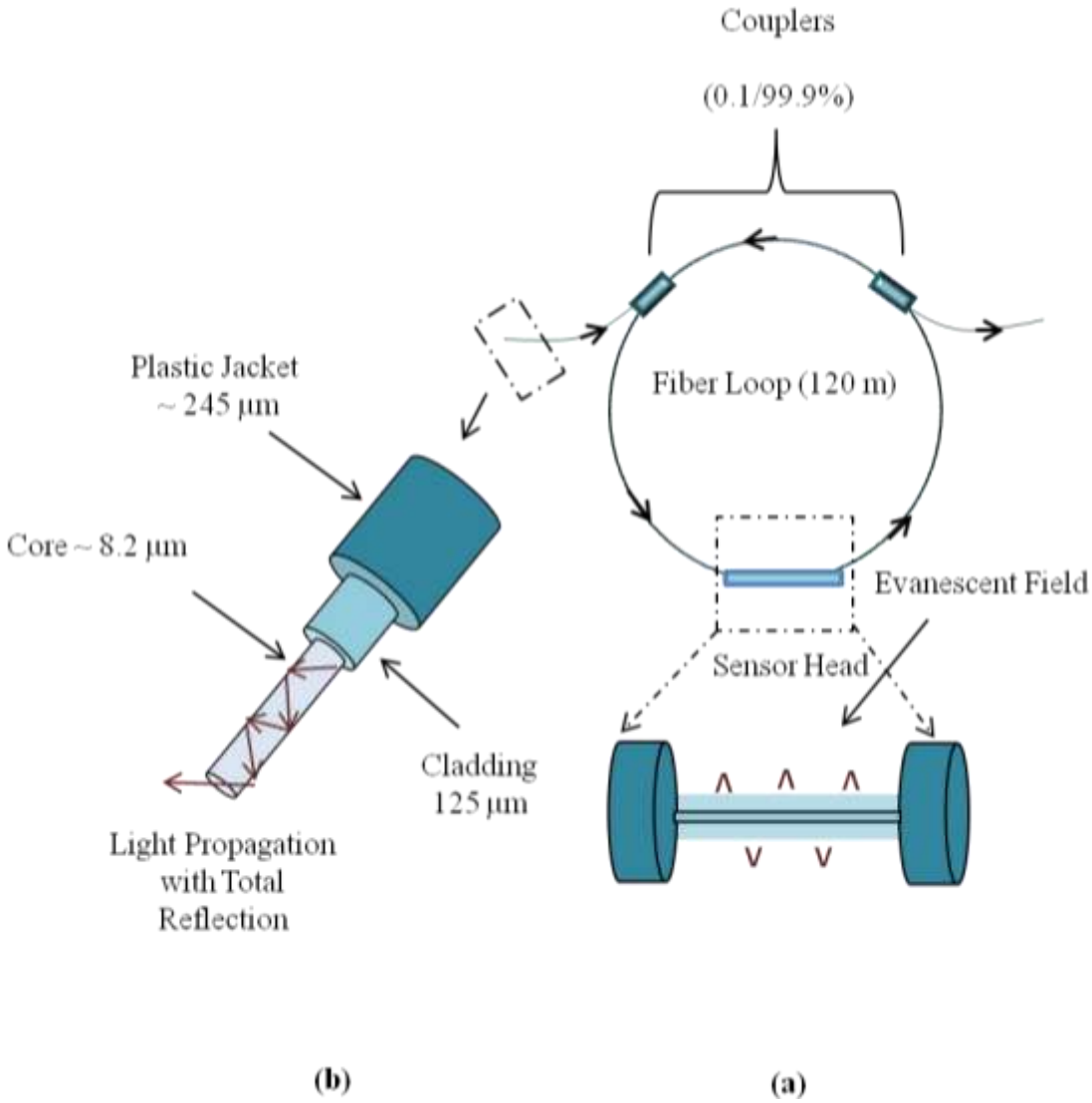

Figure 1.5 Structure of SMF and the SMF loop.

The Figure illustrates the SMF loop with the sensor head and the two couplers. (b) The structure of the SMF layers with light propagating in the core.

The total optical loss of the light in the fiber loop was estimated to be less than 0.45 dB for each fiber loop, which includes the fiber coupler's losses, absorption losses,

and fiber connectors' insertion losses. The typical value of the splicing loss was 0.02 – 0.04 dB, which was estimated by the fiber splicer.

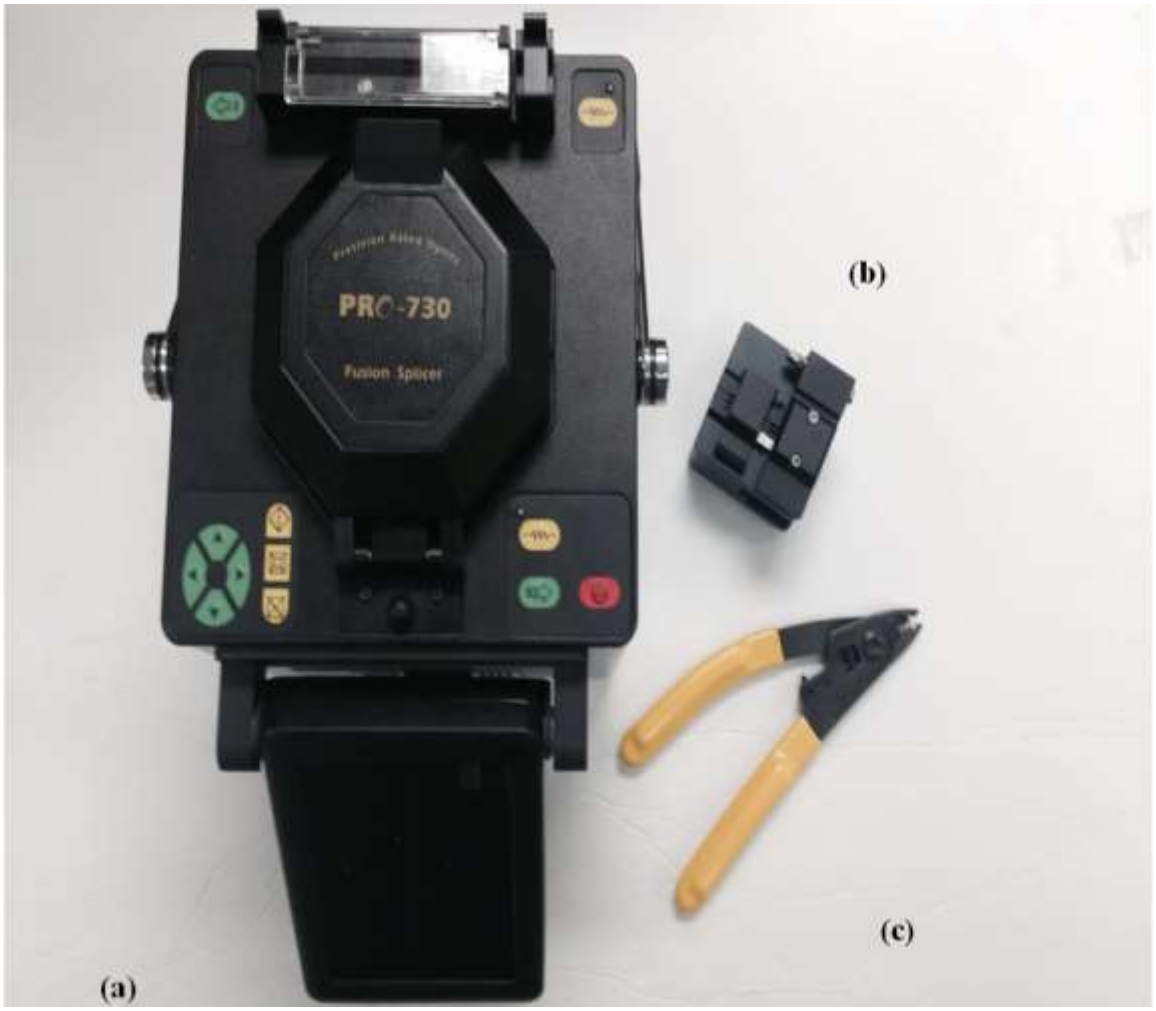

Figure 1.6 The tools to fabricate the sensor head.

(a) Fiber splicer, (b) optical fiber cleaver, and (c) Stripper

1.3.2 Continuous Wave (cw) Diode Laser Source

The EF-FLRD sensor system uses a pig-tailed distributed feedback (DFB) diode laser as the laser source. This kind of diode laser is a single mode diode laser which has a small range of tunability of ~ 2 nm – 3 nm. The DFB diode laser requires a narrow

linewidth laser beam with excellent side mode suppression with wavelength range of 760 nm to 2800 nm. The laser plate has dimensions of 500 μm × 1000 μm × 200 μm (w × L × h). The power of the DFB is in a range of 5 mW to 150 mW [45]. For example, in the DFB laser, the center wavelength of the laser diode is 1515 nm, which has a tunable range of ± 1.5 nm near the central wavelength. In this work, the DFB laser was purchased from NEL (America Inc.) [46], as shown in Figure 1.7

Figure 1.7 Image of the continuous wave laser diode.

1.3.3 Oscilloscope

An oscilloscope is used to display, to measure, and to acquire the waveform. The oscilloscope is utilized to measure the voltage as a function of time. The most common utilize of the oscilloscope is to monitor the accurate waveform of an electrical signal. In

this works, Tektronix 410A oscilloscope with a bandwidth of 400 MHz was used to monitor the signal from the photodiode detector.

1.3.4 InGaAs Detector

The InGaAs photodiode detector is used to monitor weak photosignals and short pulses. In this work, the InGaAs photodiode detector was purchased from Thorlabs (model PDA50B). The photodiode detector has a wide wavelength response range. The wavelength range of the detector is varied from the ultraviolet to the mid-infrared (150 nm to 2.6 nm). The detection range of InGaAs the photodiode detector is from 800 nm to 1800 nm, and the wide bend is a range of 0 – 10 V output [48]. The detector amplification was setup at 50 dB signal-to-noise ratio with a minimum detectible power of 10 nW. The trigger threshold was setup at 0.5 V.

1.3.5 Electronic Control

The electronic control system contains of a current controller (ILX Lightwave, LDT-5948), a pulse generator (Stanford Research System, DG 535), a temperature controller (ILX Lightwave, LDX 3220), and a computer. The photodiode detector detects ringdown signals and is triggered by the pulse generator, which generates 2.5 V amplitude of a negative square wave and a tunable frequency of 10 to 100 Hz. A pulse series is utilized to decrease the laser current to zero. The temperature of the laser diode was controlled by the temperature controller for a constant room temperature of 25 °C. The temperature is constant at 0.003 °C, which assures the device's performance and dependable measurements [49]. With integrated diode protection circuits, the laser

current driver is a high constancy and low noise current source. The range of the output current is from 0 mA to 500 mA [50].

1.4 References

1. Okamoto, K. (2010). *Fundamentals of Optical Waveguides*. Academic Press.

2. Culshaw, B., and Kersey, A. (2008). Fiber-optic sensing: A historical perspective. *Journal of Lightwave Technology*, *26*(9), 1064-1078.

3. Grattan, K. T. V., and Sun, T. (2000). Fiber optic sensor technology: an overview. *Sensors and Actuators A: Physical*, *82*(1), 40-61.

4. Thyagarajan, K. S., and Ghatak, A. (2007). *Fiber Optic Essentials* (Vol. 10). John Wiley and Sons.

5. Shelby, R. A., Smith, D. R., and Schultz, S. (2001). Experimental verification of a negative index of refraction. *Science*, *292*(5514), 77-79.

6. Palmer, M. (2006). High frequency temperature sensors for high temperature turbine monitoring. *Luna Innovations Incorporated,* 1-7. Available online at: http://www.google.com/url?sa=t&rct=j&q=&esrc=s&source=web&cd=1&ved=0CEgQFjAA&url=http%3A%2F%2Fwww.virtualacquisitionshowcase.com%2Fdocument%2F1230%2Fbriefing&ei=r8UHU-zSObKssQTS8oGoAQ&usg=AFQjCNECUESMyLgzwS3ZtMEMH-5niGaqHA&bvm=bv.61725948,d.cWc

7. Rao, Y. J. (2006). Recent progress in fiber-optic extrinsic Fabry–Perot interferometric sensors. *Optical Fiber Technology*, *12*(3), 227-237.

8. Udd, E. and Spillman, W. (2011). *Fiber Optic Sensors: An Introduction for Engineers and Scientists: Second Edition*. John Wiley and Sons. doi:10.1002/9781118014103.

9. Tracey, P. M. (1991). Intrinsic fiber-optic sensors. *IEEE Transactions on Industry Applications*, *27*(1), 96-98.

10. Patrick, H. J., Williams, G. L. M., Kersey, A. D., Pedrazzani, J. R., and Vengsarkar, A. M. (1996). Hybrid fiber Bragg grating/long period fiber grating sensor for strain/temperature discrimination. *IEEE*, *Photonics Technology Letters, 8*(9), 1223-1225.

11. Mandal, J., Shen, Y., Pal, S., Sun, T., Grattan, K. T., and Augousti, A. T. (2005). Bragg grating tuned fiber laser system for measurement of wider range temperature and strain. *Optics Communications*, *244*(1), 111-121.

12. Rao, Y. J. (1999). Recent progress in applications of in-fibre Bragg grating sensors. *Optics and Lasers in Engineering*, *31*(4), 297-324.

13. Li, L., Xia, L., Xie, Z., and Liu, D. (2012). All-fiber Mach-Zehnder interferometers for sensing applications. *Optics Express*, *20*(10), 11109-11120.

14. Lecler, S. and Meyrueis, P. (2012). Intrinsic Optical Fiber Sensor, Fiber Optic Sensors, Dr Moh. Yasin (Ed.), ISBN: 978-953-307-922-6, InTech, Available from:

    http://www.intechopen.com/books/fiber-optic-%20sensors/intrinsic-optical-fiber-sensor

15. Constantin, G. C., Perrone, G., Abrate, S., and Puscas, N. N. (2006). Fabrication and characterization of low-cost polarimetric fiber-optic pressure sensor. *Journal of Optoelectronics and Advanced Materials*, *8*(4), 1635.

16. Lujo, I., Klokoc, P., Komljenovic, T., Bosiljevac, M., and Sipus, Z. (2008). Fiber-optic vibration sensor based on multimode fiber. *Radioengineering*, *17*(2), 93-97.

17. Wang, C., Kaya, M., and Wang, C. (2012). Evanescent field-fiber loop ringdown glucose sensor. *Journal of Biomedical Optics*, *17*(3), 0370041-03700410.

18. Herath, C., Wang, C., Kaya, M., and Chevalier, D. (2011). Fiber loop ringdown DNA and bacteria sensors. *Journal of Biomedical Optics*, *16*(5), 050501-050501.

19. Wolfbeis, O. S. (2004). Fiber-optic chemical sensors and biosensors. *Analytical Chemistry*, *76*(12), 3269-3284.

20. Raatikainen, P., Kassamakov, I., Kakanakov, R., and Luukkala, M. (1997). Fiber-optic liquid-level sensor. *Sensors and Actuators A: Physical*, *58*(2), 93-97.

21. Lamb, D. W., and Hooper, A. (2006). Laser-optical fiber Bragg grating anemometer for measuring gas flows: application to measuring the electric wind. *Optics Letters*, *31*(8), 1035-1037.

22. Mohd Noor, M. Y., Khalili, N., and Peng, G. D. (2013). All-Fiber Optic Humidity Sensor Based on Photonic Bandgap Fiber and Digital WMS Detection.

23. Wang, C., and Scherrer, S. T. (2004). Fiber ringdown pressure sensors. *Optics Letters*, *29*(4), 352-354.

24. Hocker, G. B. (1979). Fiber-optic sensing of pressure and temperature. *Applied Optics*, *18*(9), 1445-1448.

25. Li, H. N., Li, D. S., and Song, G. B. (2004). Recent applications of fiber optic sensors to health monitoring in civil engineering. *Engineering Structures*, *26*(11), 1647-1657.

26. Dandridge, A. and Kirkendall, C. (2002) *Passive fiber optic sensor networks* (pp. 433-448). J. M. López-Higuera (Ed.). John Wiley.

27. Grattan, K. and Meggitt, B. (1998) Optical Fiber Sensor Technology Vol 2: Devices and Technology 2 (Berlin: Springer)

28. Frankel, M. Y., and Esman, R. D. (1995). True time-delay fiber-optic control of an ultrawideband array transmitter/receiver with multibeam capability. *Microwave Theory and Techniques, IEEE Transactions on*, *43*(9), 2387-2394.

29. Wang, C. (2009). Fiber loop ringdown—a time-domain sensing technique for multi-function fiber optic sensor platforms: current status and design perspectives. *Sensors*, *9*(10), 7595-7621.

30. Wang, C. (2014). Fiber Loop Ringdown Sensors and Sensing. In *Cavity-Enhanced Spectroscopy and Sensing* (pp. 411-461). Springer Berlin Heidelberg.

31. Waechter, H., Litman, J., Cheung, A. H., Barnes, J. A., and Loock, H. P. (2010). Chemical sensing using fiber cavity ring-down spectroscopy. *Sensors*, *10*(3), 1716-1742.

32. Wang, C., Srivastava, N., Jones, B. A., and Reese, R. B. (2008). A novel multiple species ringdown spectrometer for in situ measurements of methane, carbon dioxide, and carbon isotope. *Applied Physics B*, *92*(2), 259-270.

33. Stewart, G., Atherton, K., Yu, H., and Culshaw, B. (2001). An investigation of an optical fibre amplifier loop for intra-cavity and ring-down cavity loss measurements. *Measurement Science and Technology*, *12*(7), 843.

34. Brown, R. S., Kozin, I., Tong, Z., Oleschuk, R. D., and Loock, H. P. (2002). Fiber-loop ring-down spectroscopy. *The Journal of Chemical Physics*, *117*(23), 10444-10447.

35. Wang, C., and Herath, C. (2010). Fabrication and characterization of fiber loop ringdown evanescent field sensors. *Measurement Science and Technology*, *21*(8), 085205.

36. Wang, C. (2005). Fiber ringdown temperature sensors. *Optical Engineering*, *44*(3), 030503-030503.

37. Wang, C., and Scherrer, S. T. (2004). Fiber loop ringdown for physical sensor development: pressure sensor. *Applied Optics*, *43*(35), 6458-6464.

38. Sahay, P., Kaya, M., and Wang, C. (2012). Fiber Loop Ringdown Sensor for Potential Real-Time Monitoring of Cracks in Concrete Structures: An Exploratory Study. *Sensors*, *13*(1), 39-57.

39. Kaya, M., Sahay, P., and Wang, C. (2013). Reproducibly reversible fiber loop ringdown water sensor embedded in concrete and grout for water monitoring. *Sensors and Actuators B: Chemical*, *176*, 803-810.

40. Von Lerber, T., and Sigrist, M. W. (2002). Cavity-ring-down principle for fiber-optic resonators: experimental realization of bending loss and evanescent-field sensing. *Applied Optics*, *41*(18), 3567-3575.

41. Wang, C. and Herath, C. (2010). High-sensitivity fiber-loop ringdown evanescent-field index sensors using single-mode fiber. *Optics Letters*, *35*(10), 1629-1631.

42. http://www.corning.com/docs/opticalfiber/pi1463.pdf

43. http://www.opneti.com/uploadfile/20101127/20101127181202600.pdf

44. Herath, C. S. (2010). Fiber loop ringdown evanescent field sensors. Master Thesis, *Mississippi State University*, *MS*

45. http://www.sacher-laser.com/home/laser-diode/distributed_feedback_laser/dfb/single_mode.html

46. http://www.toptica.com/products/research_grade_diode_lasers/tunable_diode_lasers/diode_lasers_with_largest_mode_hop_free_tuning_range.html

47. http://www.tek.com/oscilloscope#all

48. http://www.thorlabs.us/NewGroupPage9.cfm?ObjectGroup_ID=947

49. http://www.newport.com/LDT-5900C-Series-laser-Diode-Themoelectric-Tempe/1009826/1033/info.aspx

50. http://www.newport.com/LDT-3200-Series-Precision-Laser-Diode-Drivers/1010347/1033/info.aspx

CHAPTER II

FIBER LOOP GAS FLOW SENSORS

Fiber loop ringdown (FLRD) is a multipurpose sensing technique. The FLRD technique has been increasingly used for developments of high sensitivity, fast response FLRD physical, chemical, and biomedical sensors. In this chapter, the first fiber loop ringdown gas flow sensor has reported. The FLRD gas flow sensor was based on the micro-bending sensing mechanism. When a gas flows through the sensor head and created a physical deformation, optical losses were induced. In this work, the sensor was used to sense airflow at various rates. Two different SH configurations were demonstrated. The results prove that the FLRD sensor has a large dynamic range of 5 to 22.5 standard liters per minute (slpm) to measure airflow, with an estimated theoretical detection sensitivity limit of 0.1 slpm. With the known of airflow cross sections that has used, the associated airflow speeds measured in this work are in the range from 5.69 m/s to 311.04 m/s. The sensor head demonstrated fast response (< 1 s) and excellent reversibility and reproducibility. Compared with other kinds of airflow FOSs, this new FLRD airflow sensor, besides its low cost and simplicity , gives the complimentary ability of measuring higher gas flow rates and has high potential of fiber optic gas flow sensor network.

2.1 Introduction

Gas and air flow measurements are of importance in several applications, such as medical applications, environmental monitoring, mechanical engineering, industrial procedure control, mine industries, etc. In the mining field, for example, ventilation underground is important to miners, since airflow in a strategic location is required to be attenuated because of the increase in gas release rate that may generate a combustible gas mixture [1,2]. Therefore, observing airflow in a mining field is desirably accomplished by a sensing technique that is electrical free and chemical. Moreover, in order to prevent a mine from a ventilation weakening or failure in airflow control or an insufficient early warning system, monitoring and measuring airflow in multiple positions in the mine is needed. Also, in many cases, a remotely-controllable, low-cost, and electrical hazards and chemical free airflow sensor network containing many sensor units with a large dynamic range is highly desired, yet such a sensor system is not presented using traditional gas flow sensing techniques.

Fiber optic sensors, because of their attractive application features, such as small footprint, low cost, immunity to electromagnetic interference, lightweight and ability to cover long distances and to be multiplexed, have been playing an increasingly significant role in the sensing community [3-7] In current years, FOSs have also begun to find their applications in the improvement of air/gas flow sensors [8-16] Different kinds of FOSs techniques, such as fiber Bragg grating (FBG) [8-13], tapered fiber Michelson interferometer [14], Fabry-Perot interferometer [15,16], *etc* have been illustrated to monitor air/gas flow sensors. For example, Cashdollar *et al*. reported nitrogen gas flow by a FBG sensor [11]. A sliver film was deposited on the surface of the FBG sensor and

employed with on the self-heated optical technique. The nitrogen gas was flowed vertically toward to the sensor, thus the Bragg wavelength shifted. The FBG sensor was able to measure nitrogen flow in a speed range from 0.35 to 2.63 m/s. Jewart *et al*. investigated another FBG sensor to monitor direction and magnitude of gas flow based on the convective heat transfer technique [9]. The sensor was created using two cross-mounted thin silver films FBG (X-probe) that was heated by using the laser light. The convective heat dissipation generating from the gas flow caused a change in the temperature of the FBG sensor, which led to a shift in the resonance wavelength of the FBG sensor. The FBG sensor measured the gas flow in range between 0.3 and 20 m/s. Gao *et al*. reported a fiber optic airflow sensor by the dual FBG technique [10] in which one FBG was utilized as a reference and the other was utilized for sensing. A laser beam was used to heat the FBG. The rate of heat loss from the FBG sensor generated from airflow was calculated from a wavelength shift. The sensitivity of the sensor dependent on the rate of the heat transmit from the sensor to the surrounding location. The sensitivity of the sensor was affected by the coatings and the pumping power. The sensitivity of the sensor was about 0.012 m/s for a flow speed in the range from 2 to 8 m/s. Similarly, Dong *et al.* was also investigating the FBG sensing approach for sensing airflow [11]. This FBG sensor monitored airflow with a sensitivity of 6 m/s. Most recently, Wang *et al*. investigating a hot-wire airflow sensor by a FBG coated by a silver film as the sensor [12]. The sensor was able to measure a range between 0 and 13.7 m/s with a sensitivity of ~ 0.0017 m/s. Yun *et al*. have demonstrated a fiber optic airflow sensor based on a distributed Bragg reflector [13]. The airflow speed was converted to a vertical force that led to change the fiber birefringence. Thus, the beat-frequency of the

distributed Bragg reflector changed. The sensor measured an airflow velocity in a range of 8 to 40 m/s.

In the above-mentioned, the FBG sensors measure the air/gas flow speed based on a wavelength shift while tapered fiber Michelson and Fabry-Perot interferometer sensors measure the air/gas flow speed based on the interferometer, which can be sensed by a fiber that is traveling during the flow section. Therefore, the air/gas flow bends or distorts the fiber to disturb the interference pattern. For example, Lee *et al*. [14] reported an airflow sensor to monitor a micro-flow rate up to 1.2 m/s by by an air-gap Fabry-Perot interferometer. Also, the same group reported another airflow sensor based on a pendulum kind of anisotropic flat-clad tapered fiber Michelson interferometer [15]. The air was flowed in various directions toward to the sensor, which led to create a force on the fiber pendulum. The force generated bending on the sensor, thus the interference fringes were shifted. Interference spectra was measured by an optical spectrum analyzer when the airflow speed was increased, the wavelengths were shifted to shorter interference fringes the sensitivity of the sensor depended on the diameter and length of the fiber cantilever. The sensor measured airflow in the range from 0 to 2 m/s. Sadegh *et al*. [16] demonstrated an airflow sensor by a micro Fabry-Perot (FP) cavity containing a micro-cantilever and a fiber, which was fabricated using a photolithography technique. The airflow generated defection in the micro-cantilever, thus the cavity length of the FP caused a change that made the fringe to shift. The minimum detectable of airflow speed sensor was 0.05 m/s.

In this chapter, a fiber loop ringdown (FLRD) technique has been explored for airflow (AF) sensing. FLRD is a highly-sensitive fiber optic sensing technique, which is a

time-domain technique [e.g., 5, 17,18]. The concept of the FLRD technique was first established by Stewart *et al*. via a double-loop configuration [19]. Today, the simple meaning of FLRD is a simplified fiber loop ringdown, using a single fiber loop [e.g., 20]. In FLRD, a beam pulse is injected into a fiber loop and travels inside the loop for many round trips. During each round trip, a small fraction of the beam pulse is injected out of the fiber loop into a detector by a fiber coupler, and the remains of the light keeps traveling in the fiber loop, experiencing inside fiber transmission losses. A signal is observed by the detector and typically follows a single exponential decay after each round trip. The exponential decay time constant is identified as the ringdown time that is the sensing signal of the FLRD technique. A longer ringdown time is associated with a slower decay rate that means a lower optical loss of the beam in the fiber loop, and vice versa. To date, the FLRD technique has been demonstrated for multi-function fiber optic sensor developments, including physical, chemical, and biomedical sensors. These sensors have been described in several recent reviews [5,17,18]. In this chapter, a new airflow (AF) sensors based on the FLRD technique were reported. The FLRD-AF sensor has been illustrated by sensing an AF rate up to 22.5 slpm. The FLRD-AF sensor head (SH) contained a part of partially-etched single mode fiber (SMF). Two different airflow SH configurations were demonstrated. The FLRD-AF sensors using both SH configurations offered fast response and excellent reversibility and reproducibility.

2.2 Experimental Setup

2.2.1 The FLRD System and Fabrication of the Sensor Heads

Figure 2.1 demonstrates the schematic diagram of the FLRD technique. The FLRD technique contained two main parts: a sensor unit and a sensor control system. The

FLRD sensor unit contained a single mode fiber loop (SMF 28, Corning, Inc) linked to two identical 2 × 1 fiber couplers (Opneti Communication Co., Hong Kong). A small piece in the middle of the fused silica SMF, i.e., 3 - 6 cm, was fabricated as a SH. The control system contained a photodiode detector (Thorlabs, PDA50B), a continuous wave (cw) diode laser (NTT electronics), and laser control electronics, such as a current driver and a diode laser temperature controller. In addition, the disconnection and connection of the sensor from the control system can be done by two single mode fiber FC/APC connectors. The laser diode wavelength was fixed at 1515.25 nm.

The diameter of the optical fiber core and cladding were ~ 8.2 μm and 125 μm, respectively. The optical fiber loop total length of was 120 m. At the two-leg end, the two identical 2 × 1 fiber couplers were fabricated with a split ratio 0.1:99.9. The total optical loss of the light in the loop included fiber connectors' insertion losses, absorption losses, and fiber coupler's losses. The total optical loss was estimated to be < 0.45 dB for each fiber loop. The fiber splicer (Fusion Splicer, PRO 730) was used to estimated the splicing loss with a typical value of 0.02 to 0.04 dB. Once a light source was injected into the fiber loop, the detector observed a ringdown signal. Then, the signal was fed to a pulse generator (SRS, DG 535) to produce a series of the negative square waves. These pulsed square waves were applied to the current driver to decrease the laser current to zero rapidly, and the continuous wave diode laser produced a series of laser pulses. For each laser pulse, the detector observed a series of pulsed spikes. The envelope of the pulse spikes created a single exponential decay, from which a ringdown time was found. More details about a FLRD sensor scheme can be seen [i.e., 21,22].

The etching process to produce a SH was illustrated in recent publications [23-25]. The plastic jacket was removed from a part of the SMF with various lengths, i.e., 3 - 6 cm. For the etching process, the part was fully immersed into a 48% hydrofluoric acid (HF) solution for proximately 34 min. The etching process was continuously watched by monitoring changes in ringdown time [26].

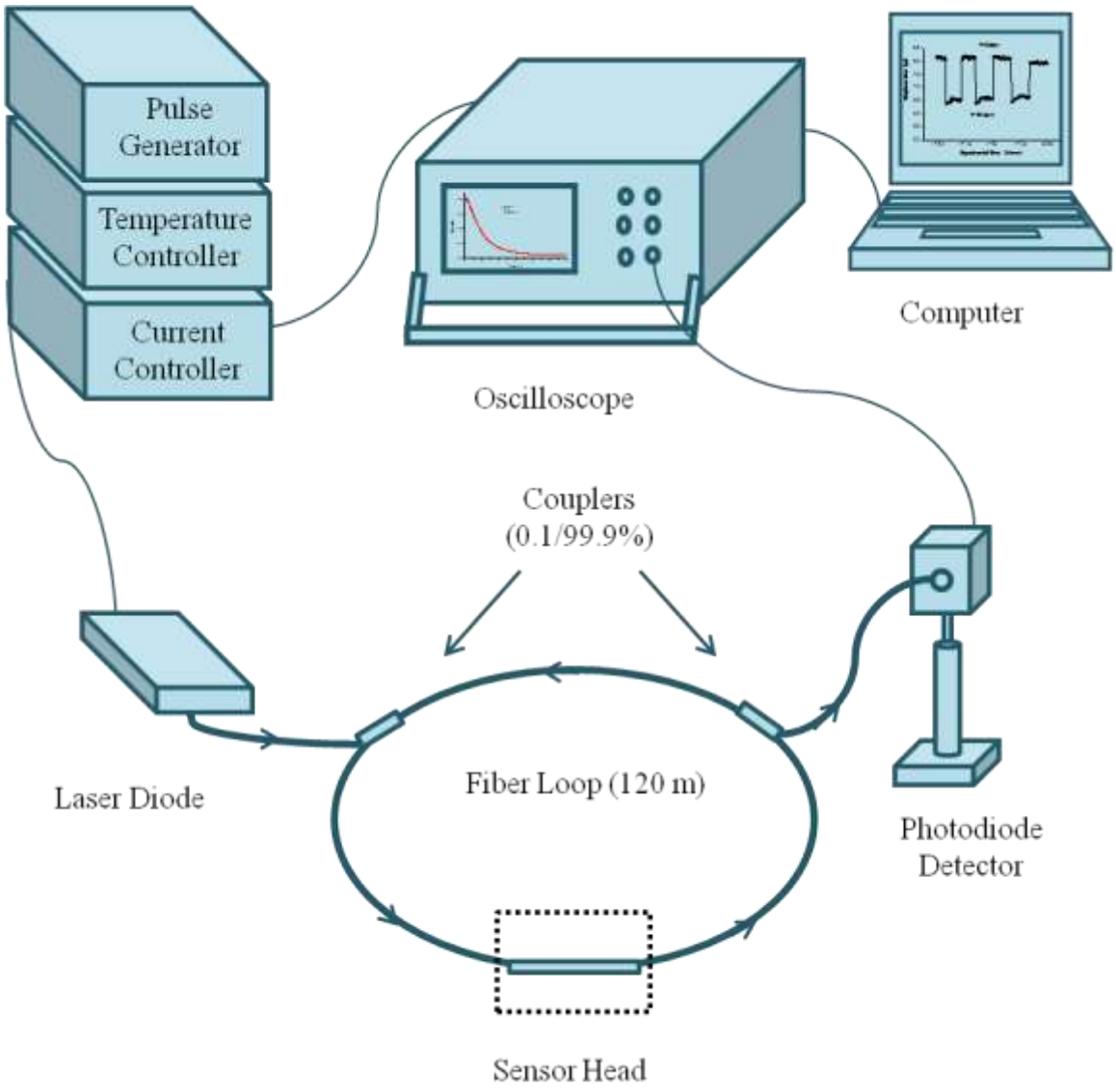

Figure 2.1 Illustration of a FLRD sensor system.

2.2.2 Configuration of Sensor Head

Figure 2.2 and 2.3 illustrate two different configurations of the airflow SH. The first configuration represents a horizontally configured AF SH, as shown in Figure 2.2. The SH was sited horizontally. The two ends of the sensor head were fixed on the top of a metal ring. The metal ring was used as a fiber supporter only. An AF source was installed vertically from the top of the center of the SH. The AF source was directly applied to the SH for measurement. A flow meter with an AF range of 0 to 22.5 slpm was used to control the AF source. Figure 2.2 demonstrates the horizontally configured AF sensor head, where *d* is the tube diameter of the AF source nozzle, *D* is the shortest distance between the SH and the AF source nozzle (with an estimated distance of 0.5 cm), and *l* is the length of the SH, (6 cm long). When the AF source was turned on, a force was created vertically onto the SH and caused micro-bending [e.g., 27,28]. Thus, with an increase in the AF rate, the optical loss of the fiber loop was increased. Different tubes with various AF nozzle diameters, i.e., 0.58, 1.27, and 4.32 mm, were used. Each AF tube had a various AF velocity, as listed in Table 2.1. The flow rate was converted to velocity using Equation (2.1)

$$V = \frac{F}{a} \tag{2.1}$$

where V represents the velocity, F is a flow rate (m^3/s), and a is a cross section of the tube ($r^2 \pi$) which r is radius.

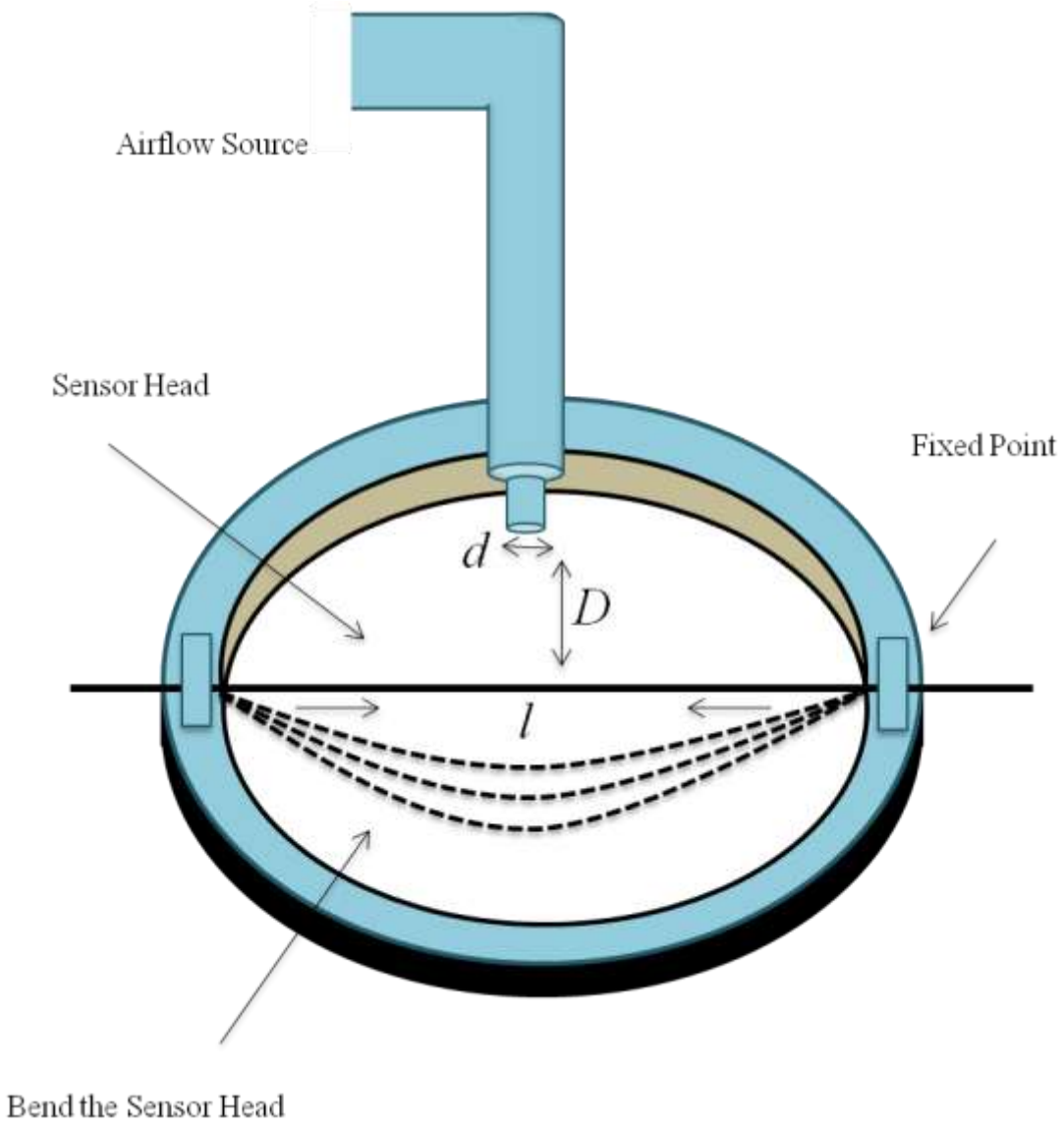

Figure 2.2 Illustration of the airflow sensor horizontal head configuration.

Table 2.1 Different airflow rates create different flow speeds via using flow nozzles of different diameters, such as $d_1 = 0.58$ mm, $d_2 = 1.27$ mm, and $d_3 = 4.32$ mm

Flow rate (slpm) of the airflow source	Diameter (mm) of the airflow nozzle	Velocity (m/s) calculated from the flow rate
5	d_1	311.04
	d_2	65.81
	d_3	5.69
7.5	d_2	98.72
	d_3	8.54
10.0	d_2	131.63
	d_3	11.38
12.5	d_2	164.54
	d_3	14.23
15.0	d_3	17.08
17.5	d_3	19.92
20.0	d_3	22.77
22.5	d_3	25.62

The second configuration illustrates the vertical SH configuration, as shown in Figure 2.3. The SH (one part of partially-etched SMF) was placed vertically by fixing one end of the SH. The other end was spliced to one part of SMF, which was passed through the center a spherical plastic bead with diameter of 6.2 mm and a weight of 124.5 mg. The entire part (SH) from the top fixing point to the end of the SMF was spliced into the other part of a ringdown fiber loop (Figure 2.1). The AF source was inserted toward the bead, as shown in Figure 2.3. When the AF source was injected vertically from the bottom of the bead, the air pushed the bead up and created micro-bending in the SH. Due to the gravity, the bead fell down once the AF source was shut down

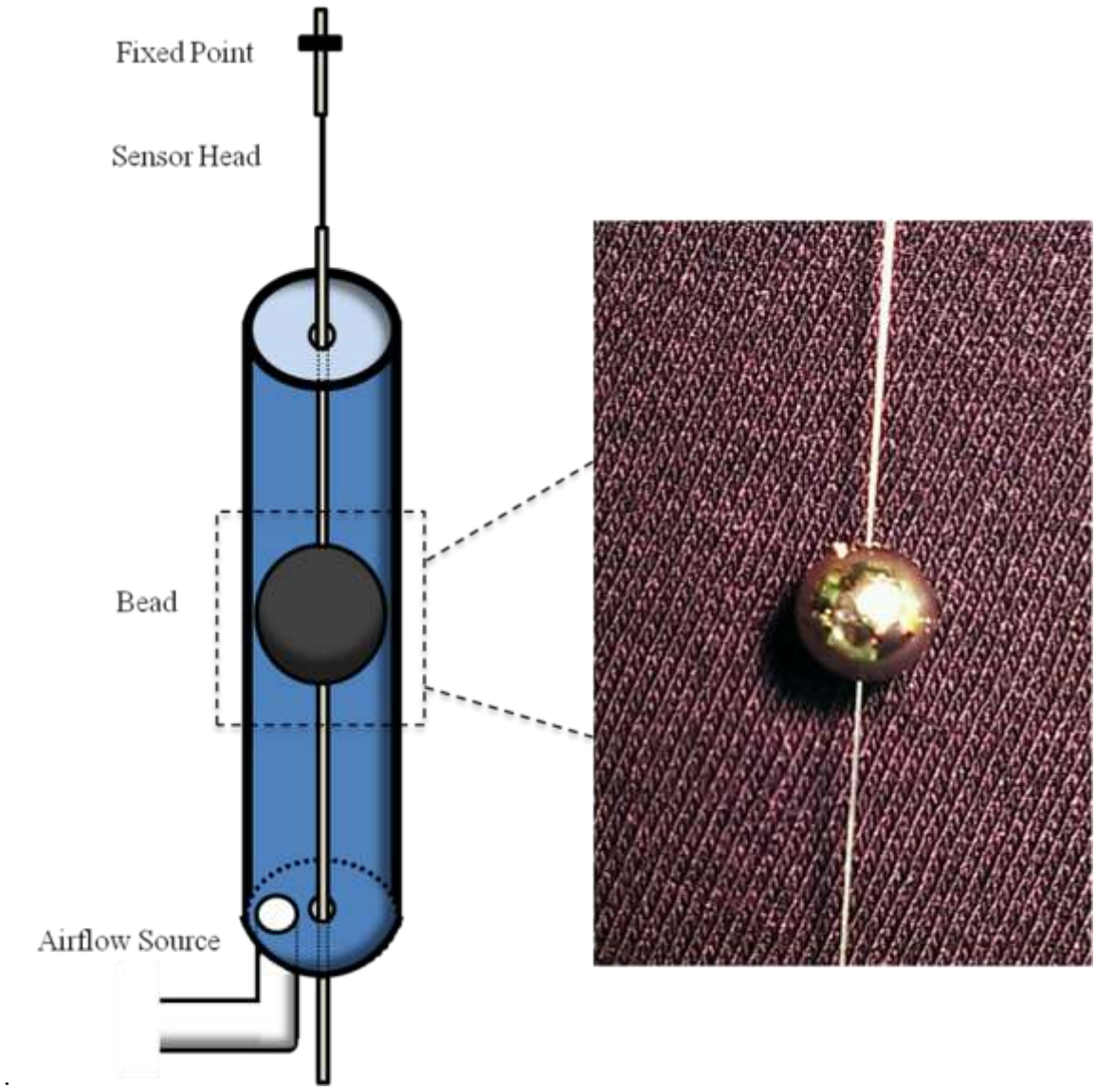

Figure 2.3 Illustration of the AF vertical sensor head configuration.

2.3 FLRD-AF Sensor's Principle

A beam pulse is coupled into a fiber loop and travels for many round trips inside the loop. In each round trip, the intensity of the beam pulse decreases due to the inner optical loss. From each round trip, the detector observed the transmitted light with

different intensities. Therefore, the change of the light intensity as observed by the detector can be written as [21]

$$\frac{dI}{dt} = -\frac{IAc}{nL} \tag{2.2}$$

where I is the beam pulse intensity at time t (the time is zero when the beam pulse is coupled into the loop and the beam pulse shuts down), c is the speed of the light in vacuum, L is the total length of the fiber loop, n is the fiber loop reflective index, and A is the total transmission loss of the loop of the light pulse per one trip (in decibel (dB)). Solution of the Equation (2.2) illustrates the temporal behavior of the light intensity I observed by the detector as expressed in Equation (2.3)

$$I = I_0\, e^{-\frac{c}{nL}At} \tag{2.3}$$

The time for the beam intensity I to decrease to $\frac{1}{e}$ of the initial beam intensity, I_0, is termed as the ringdown time, τ_0, and can be given in Equation (2.4)

$$\tau_{0=\frac{nL}{cA}} \tag{2.4}$$

$$\tau = \frac{nL}{c(A+B)} \tag{2.5}$$

For a given FLRD sensor, the total transmission loss A can be defined by the physical parameters of the sensor unit, such as the reflective index, the fiber absorption loss, the couplers' insertion losses, and the fiber loop length. In addition, the total transmission losses for a given fiber loop keeps constant. With an exterior action, e.g. a sensing activity exists at the part of the fiber loop (SH), the effect is an additional optical

loss B of the light in the fiber loop, and this causes a change in the ringdown time, τ, given in Equation (2.5). From Equations (2.4)) and (2.5), we achieve

$$B = \frac{nL}{c}\left(\frac{1}{\tau} - \frac{1}{\tau_0}\right) \tag{2.6}$$

Equation (2.6) illustrates the principle of FLRD. The additional optical loss, B, is defined by monitoring the ringdown time τ_0 without the sensing activity and the ringdown time τ with the activity. In this chapter, the sensing activity was airflow, which was introduced in the two various configurations. First, the relationship between the ringdown signal and the AF rate was investigated. Assume a small micro-bending appears on the surface of the SH after the AF source is turned on. Because the AF creates micro-bending that occurs in the partially-etched SMF, the total optical loss, B, can be written as δF, where δ is the loss per unit volumetric flow rate and F is the flow rate. Thus, the optical loss, B, causes a change in the ringdown signal, so that becomes

$$\tau = \frac{nL}{c(A+ \delta F)} \tag{2.7}$$

From Equations (2.6) and (2.7), the optical loss can be written as

$$\left(\frac{1}{\tau} - \frac{1}{\tau_0}\right) = \frac{c}{nL}\, B = \frac{c\delta F}{nL} = KF \tag{2.8}$$

where $K = c\,\frac{\delta}{nL}$ Equation (2.8) illustrates a linear relationship between the flow rate F and $\left(\frac{1}{\tau} - \frac{1}{\tau_0}\right)$, with K as a constant.

2.4 Results and Discussion

2.4.1 The FLRD-AF Sensor with the Horizontal Sensor Head Configuration

2.4.1.1 The Sensor's Response to the Same Flow Rate

Figure 2.4 shows a typical response curve of the FLRD sensor with the horizontal SH configuration. In Figure 2.4, the applied AF was fixed at a flow rate of 5 slpm that was converted to a flow speed of 311.04 m/s, given the diameter of the flow nozzle of 0.58 mm. From points *A* to *B*, the data was recorded without AF events, and the ringdown time through this period was 14.5 μs. At point *B*, the airflow source was turned on with a flow rate of 5 slpm. From points *C* to *D,* the AF was kept flowing continuously, and the monitored ringdown time at this flow rate was 14.1 μs. The vertical drop lines shown in the data show the fast response of the sensor to the change of optical losses generating from the change in AF in the sensor. In addition, when the AF rate was switched between 0 and 5 slpm, the responses of the sensor were reproducible, as shown in Figure 2.4. Averaging over 100 ringdown times, which mean 100 sensing events, the airflow sensor's response to the airflow event was near real-time, ~1 sec.

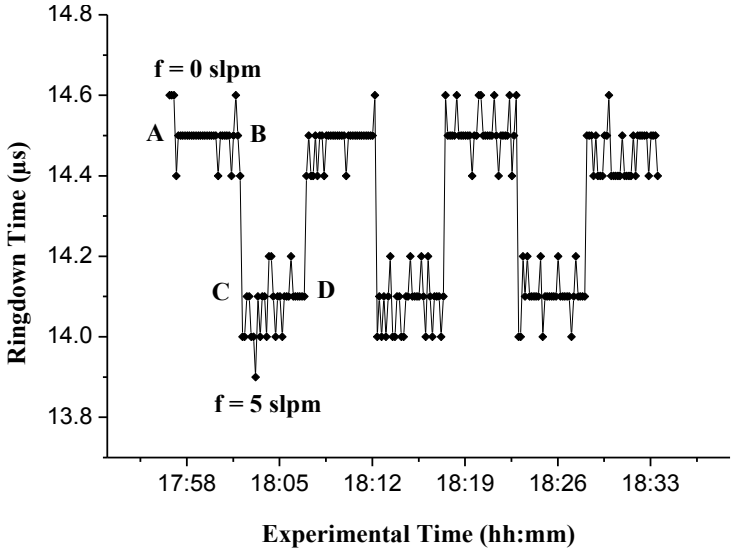

Figure 2.4 Reproducible response of FLRD-AF sensor with the horizontal SH configuration at fixed AF rate of 5 slpm.

2.4.1.2 FLRD-AF Sensor's Response to Different Flow Rates

Figure 2.5 (a-e) illustrates typical responses of the FLRD-AF sensor with the horizontal SH configuration to different AF rates. The x-axis indicates the actual experimental time (hour: minute). The stepwise signals in Figure 2.5(a-d) were monitored from examined different AF rates in different AF variation patterns, e.g., starting with a low flow rate and progressively increasing to a high flow rate and then decreasing to zero flow, or in reverse order, etc. The applied AF in Figure 2.5(a-c) was from 0 to 12.5 slpm that was converted to flow velocities in the range of 0 to 164.54 m/s, known the diameter of the flow nozzle of 1.27 mm. In Figure 2.5(a), during points *A* to *B*, the ringdown time was calculated to be 11.7 µs when no external AF was applied to the sensor head. At point *B*, the AF was turned on and kept at a stable flow of 5 slpm from point *C* to point *D*; the ringdown time was measured at 11.5 µs. From point *E* to point *F*, the AF was

increased to 7.5 slpm, and the monitored ringdown time was 11.1 μs. In the same way, further increase in the AF to 10 slpm for the period of *G* - *H* and 12.5 slpm for the period of *I* - *J*, the observed ringdown times were 10.8 μs and 10.6 μs, respectively. The consequence from points *C* to *J* showed that the ringdown time decreased with increase of the AF as a consequence of more micro-bending occurring on the SH. Once the AF source was shut down, the ringdown time speedily increased back to the origin baseline. This behavior was because of no force acting on the SH; therefore no micro-bending was produced.

Figure 2.5(b) illustrates the response of the FLRD sensor when it was applied a higher AF first and then at gradually decreasing flow rates, a reversed testing process to the one given in Figure 2.5(a). The sensor's response changed from 11.8 μs to 10.7 μs and went back to the baseline 11.7 μs in the flow range from 0 to 12.5 slpm. The sensor's bi-directional response and its reproducibility were further illustrated in Figure 2.5(c). In this situation, the FLRD-AF sensor was examined by using a lower AF to a higher AF, and then the AF was symmetrically and gradually reversed back to zero flow. As a result, the FLRD-AF sensor illustrated an excellent reversible response to the airflow changes in one full cycle.

By extending the range of airflow, higher AF measurement was achieved by increasing the AF step-by-step from 0 to 22.5 slpm and then decreasing to the origin. Results are illustrated in Figure 2.5(d). The corresponding velocities were in the range from 0 to 25.62 m/s. The observed ringdown times changed from 11.8 to 10.2 μs and back to 11.8 μs. Figure 2.5(e) demonstrates the reproducible response of the FLRD sensor at the fixed high AF rate of 22.5 slpm. A decrease in ringdown time from 11.8 to

9.9 μs was monitored from zero flow to an AF of 22.5 slpm. The largest change in the ringdown time at the AF rate of 22.5 slpm showed that more micro-bending appeared on the SH. At each AF rate, the ringdown time remained stable and consistent. This exam (Figure 2.5(e)) illustrates that the SH (partially-etched bare SMF) has a reproducible physical tolerance even when it is subject to severe micro-bending, as compared to the reproducibility exam with less micro-bending (Figure 2.4).

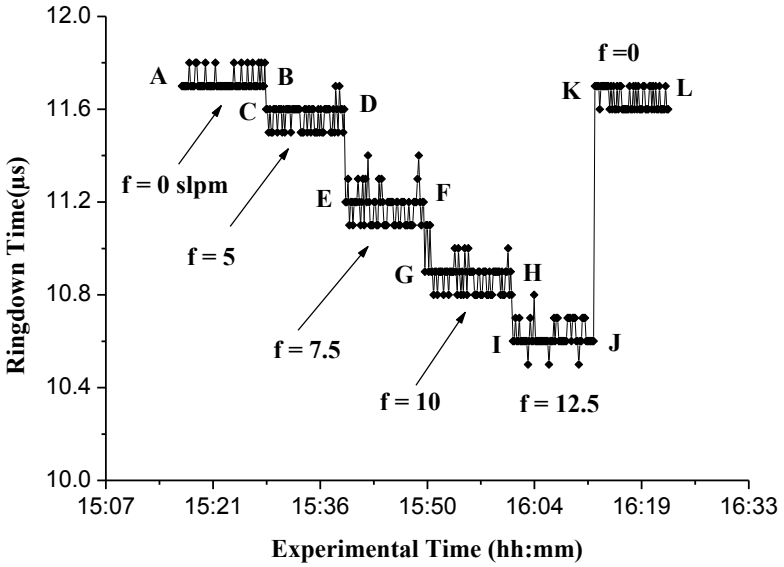

(a)

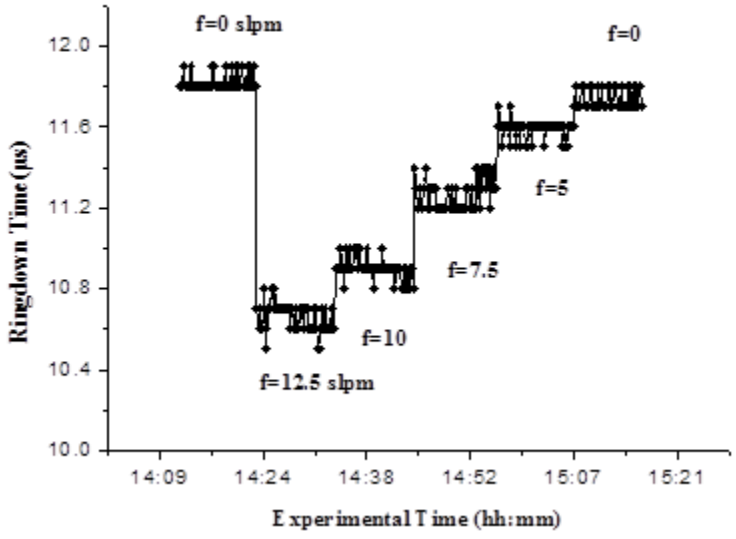

(b)

Figure 2.5 Response of the FLRD-AF sensor with the horizontal sensor head configuration to different AF rates applied in various patterns determined in this work.

(a) AF rate changes from 0 to 12.5 slpm with an increase step of 2.5 slpm and back to 0. (b) AF rate changes in a reverse procedure of the one used in (a). (c) AF rate changes in one symmetrically full cycle with a step of 2.5 slpm. (d) AF rate changes in a larger range of 0 – 22.5 slpm. (e) Reproducible physical tolerance of the sensor at the highest AF rate of 22.5 slpm examined in this work

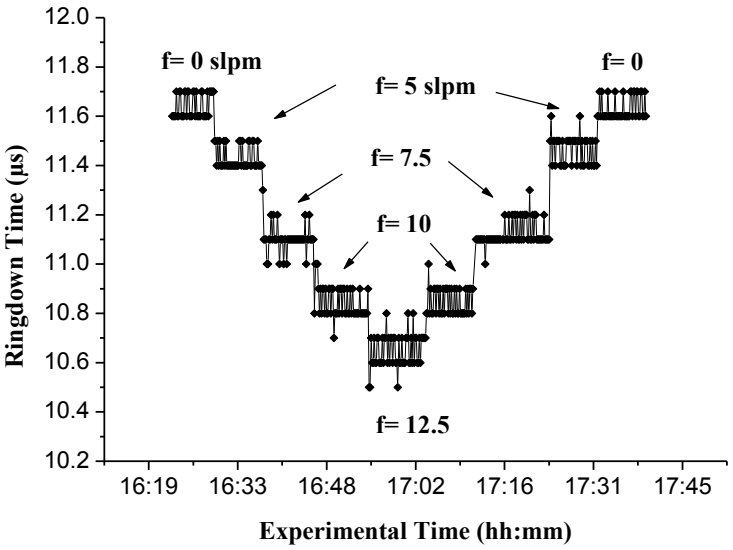

(c)

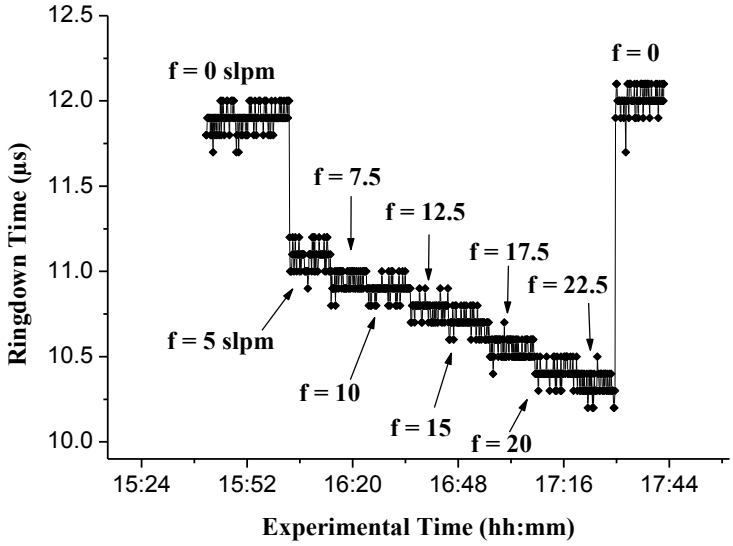

(d)

Figure 2.5 (continued)

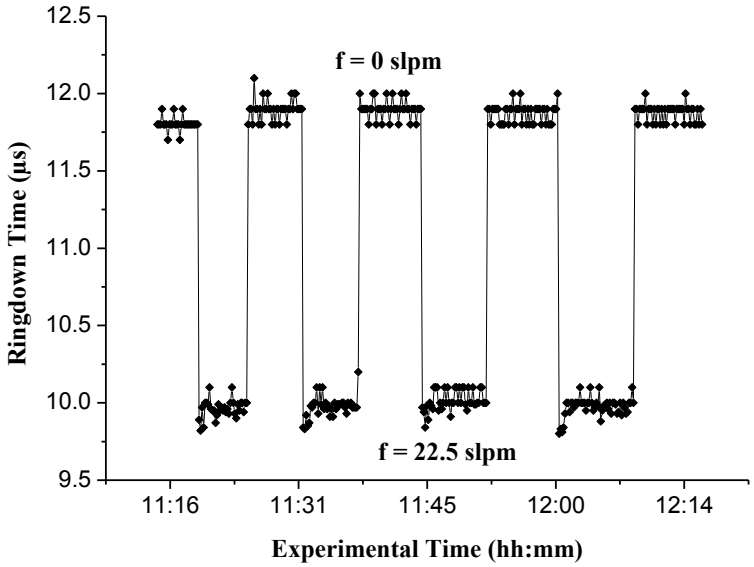

(e)

Figure 2.5 (continued)

2.4.2 The FLRD-AF Sensor with the Vertical SH Configuration

Figures 2.6(a) and (b) illustrates the response of the FLRD sensor with an SH of the vertical configuration. Figure 2.6(a) shows the response of the FLRD-AF sensor to change in the AF from 0 to 7.5 slpm, the observing ringdown times were 8.2 µs and 7.6 µs, respectively. Once a higher AF rate, 10.0 slpm, was applied to the FLRD-AF sensor, the ringdown time without and with the AF were 8.2 µs and 6.5 µs, respectively, as seen in Figure 2.6(b). Consequently, even with the vertical configuration, the FLRD-AF sensor had ability to detect AF and the consequences remained consistently repeatable.

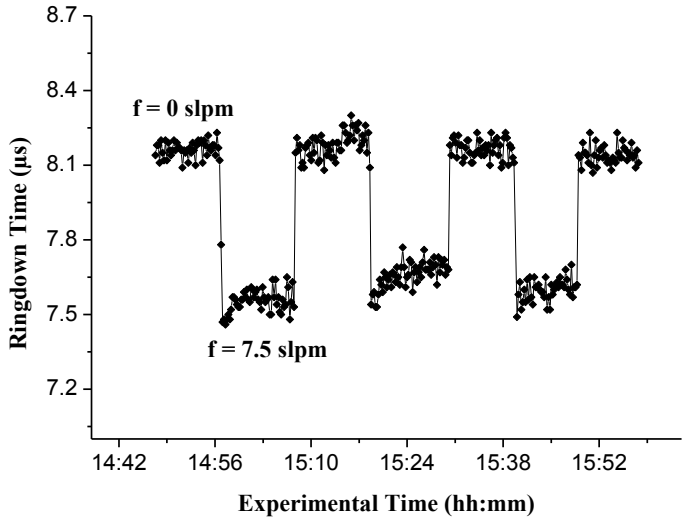

(a)

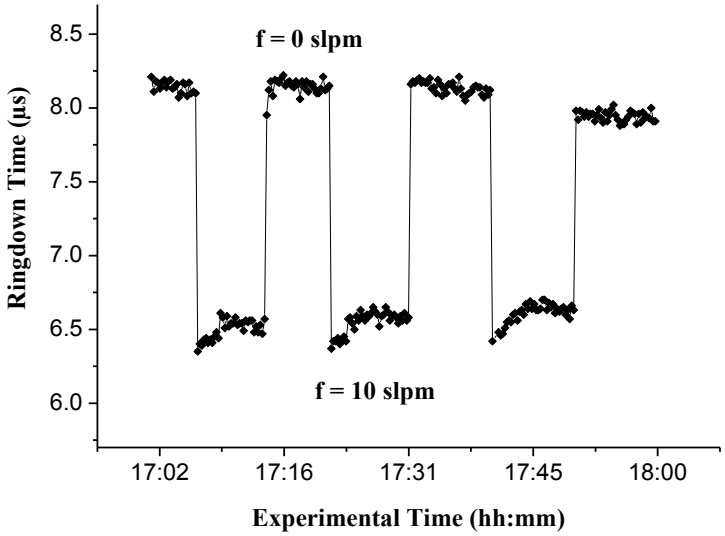

(b)

Figure 2.6 Response of the FLRD-AF sensor with the vertical SH configuration to different AF rates.

(a) AF rate = 7.5 slpm and (b) AF rate = 10 slpm

In term of sensitivity, both sensor head configurations have similar sensitivity. As an example, sensors with the two different sensor head configurations were compared when both sensors were subjected to an AF rate of 7.5 slpm. The response of the FLRD

sensor with a vertical sensor head was a change in ringdown time from 7.6 μs to 8.2 μs, when AF rate changed from 7.5 to zero slpm, as seen in Figure 2.6(a). This alteration in ringdown time corresponded to a change in the optical loss *B* of 5.8E-03 (a.u.). In the same way, as seen in Figure 2.7, the sensor with a horizontal sensor head had a change in *B* of 5.2E-03 (a.u.). The variation is a factor of 1.1. Note, this comparison was a rough estimate, because the two sensor heads did not have exactly the same physical parameters, e.g., etched fiber diameter and etched fiber length, which also define the two different sensor baselines. Consequently, it was only proved that both SH configurations were of high reversibility, reproducibility and fast response. The idea behind the vertical SH configuration was to investigate the potential of constructing a FLRD-AF meter with a comparable instrumental fashion to the commercial gas flow meters.

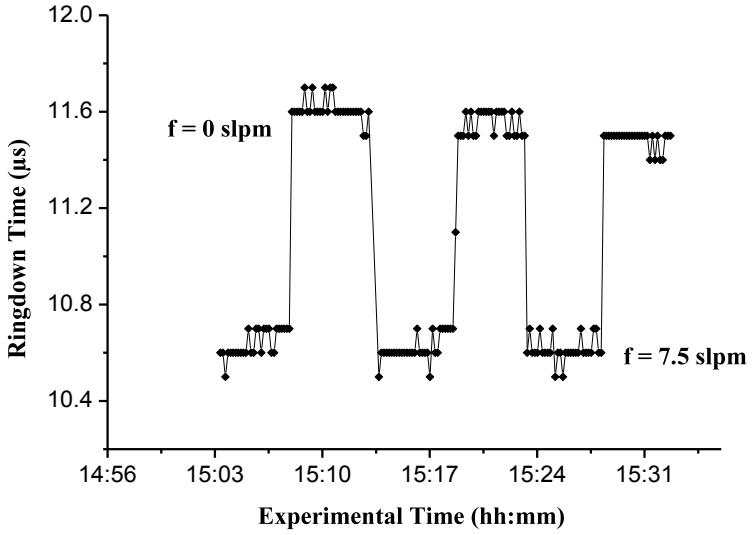

Figure 2.7 Response of a FLRD-AF sensor with the horizontal sensor head configuration to AF rate of 7.5 slpm.

2.5 Detection Sensitivity Limit Of FLRD-AF Sensors

The detection sensitivity of the FLRD airflow sensors can be determined by the sensor's baseline stability. The baseline stability of the airflow sensor is determined as σ_τ / τ where σ is one standard deviation of the ringdown time and τ is the average of the ringdown time [22]. A baseline stability of the FLRD-AF sensors studied in this work was 0.2 % by averaging over 100 ringdown events. Choosing the data in Figure 2.6(b) as an example, the change in ringdown time was 1.7 μs after the airflow rate changed by 10 slpm. With respect to the 0.2% baseline noise from the baseline ringdown time 8.2 μs, the ringdown time is 0.016 μs. Thus, a theoretical detection sensitivity limit of the FLRD-AF sensor is 0.1 slpm.

The linearity of the response of the FLRD airflow sensors to airlfow rate was tested by using one set of the data, e.g,. from Figure 2.5(c) as an example. Figure (2.8) illustrates the linearity of the FLRD sensor's response by fitting the calculated optical loss *B* in Equation (2.7) versus the AF rate. The linear relations in Figures 2.8(a) and 2.8(b) were achieved from the data given in the left-hand (increasing AF rate) and the right-hand (decreasing AF rate), respectively, of the curve in Figure 2.5(c). In Figure 8, both fitting lines illustrate good linearity, and the fitting slopes are approximately the same. Furthermore, the consequence from Figure 2.8 not only demonstrates the linearity, but also illustrates the sensor's reversibility and repeatability. In the two fittings, small nonzero intercepts are attributed to measurement uncertainty and nonzero detection activation limits of the airflow sensors. For instance, when the very low airflow, e.g., 2.5 slpm, was applied to the sensor head, the sensor was not responsive that meant the applied airflow was not high enough to activate the FLRD sensor. However, when the

sensor was activated, e.g., after applying an AF of 5.0 slpm, the sensor can distinguish an airflow rate difference of 2.5 slpm that was considered the experimental detection sensitivity limit of the sensor. It seems that, this experimental limit is far higher than the estimated theoretical limit of 0.1 slpm. Future work in the mechanical design of the SH and AF injection configuration could optimize the experimental detection sensitivity limit and this effort is under way.

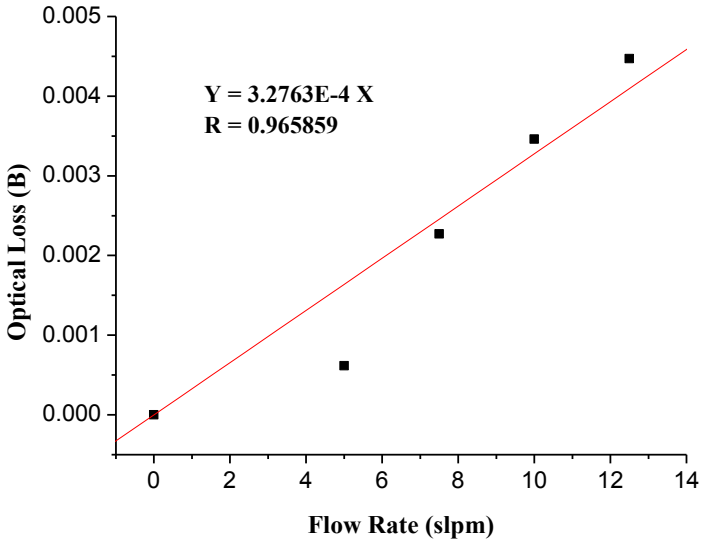

(a)

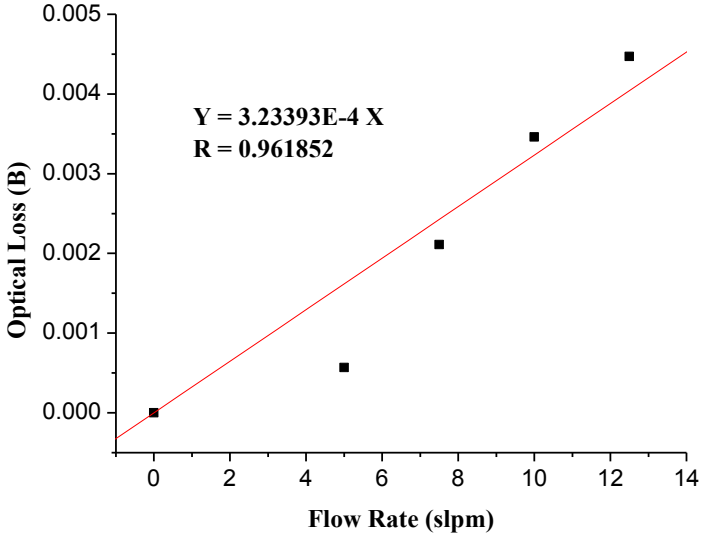

(b)

Figure 2.8 Linear response of FLRD airflow sensor to the airflow rate.

(a)and (b) Correspond to the responses given in the left part and the right part of Figure 5(c), respectively.

2.6 Comparison of Different Airflow Sensing Techniques

In addition to the fiber-based airflow techniques, there are numerous non-fiber-based air/gas flow sensing techniques, including micro-electro mechanical system

(MEMS) [29], vibration amplitude measurement method [30], micro-machined piezo-resistivity [31], etc. For instance, Wang *et al.* investigated AF measurements based on a free-standing micro-cantilever sensor using an MEMS technique [29]. A thin film of silicon nitride was coated on a silicon wafer and followed by a platinum layer. When air flowed through the cantilever structure, the beam was bent in the downward direction that caused a variation in the cross sectional area of the platinum resistor. The sensor measured a high airflow velocity up to 45 m/s. Moreover, one of the early studies related to detecting airflow was based on a vibration amplitude measurement technique [30]. The sensor was created by using a flexibly printed circuit board method. The AF was moving toward the sensor; therefore the amplitude of the vibration-induced resistance was changed. The change increased once the airflow velocity increased. The sensor was able to measure airflow in a range of 5 to 16 m/s. Another AF sensor was based on micro-machined piezo-resistivity by laser micromachining [31]. Air was flowed during a micro-tuft which generated deformation of the beam structure; therefore induced a strain in a piezo-resistor. In their work, they examined the sensor with a wind tunnel in a range between 0 and 25 m/s.

Table 2.2 summarizes the AF sensing techniques that have been explored earlier. Major sensing features of the sensors, such as the sensitivity, dynamic range, complexity in fabrication, and possible instrument cost, are listed in the table 2.2 for a rough comparison. Note, the sensors listed in Table 2.2 are not inclusive though an exhaustive search has been done. The highest sensing sensitivity of the sensors recorded is 0.0017 m/s [12] that is far more sensitive than the sensitivity (2.9 m/s) of the FLRD-AF sensors studied in this work. However, in term of sensing dynamic range, the FLRD airflow

sensors have a significantly larger dynamic range, e.g., 5.7 m/s to 311.0 m/s, with the highest limit of 311.0 m/s. This characteristic is advantageous in some applications where sensing a high airflow rate or flow velocity is needed. Moreover, the FLRD airflow sensor does not use a delicate fiber optical component, e.g. a FBG, a micro-interferometer, or MEMS; the SH is a part of partially-etched SMF that is very inexpensive. In addition to this low cost and simplicity, comparatively, the FLRD airflow sensor is insensitive to environmental temperature, since SMF, different than FBGs, has an extremely low thermal coefficient. This feature allows FLRD airflow sensors to be able to stay alive in harsh environments, e.g., large differences of surrounding temperature. In conclusion, because of the nature of the FLRD signal [5], time, the FLRD airflow sensors have high potential for sensor multiplexing to accomplish multiple-spot AF sensing in a single sensor network.

Table 2.2 Summary of air/gas flow sensors that are categorized by non-fiber optics-based or fiber optics-based techniques

Air/gas Flow Sensors	Sensing Technique	Sensing Function (air/gas)	Dynamic Range (m/s)	Sensitivity (m/s)	Fabrication Complexity	Cost[c]	Ref.
Fiber Optics-Based	FBG, Self-Heated Optical Hot Wire	Nitrogen gas flow	0.35 - 2.63	0.35	Simple	High	8
	FBB, Convective Heat Transfer Method	Gas flow	0.3 – 20	< 0.3[a]	Complex	High	9
	Dual FBG Technique	Airflow	2 – 8	0.012	Complex	High	10
	FBG, Thermal Anemometry	Airflow	0 – 6	6	Simple	High	11
	FBG, Hot-Wire Anemometer	Airflow	0 – 13.7	0.0017	Simple	High	12
	Distributed Bragg Reflector	Airflow	8 - 40	< 8[a]	Complex	High	13
	Fabry-Perot Interferometer	Airflow	0 - 1.2	33.17	Complex	High	14
	Michelson Interferometer	Airflow	0 - 2	< 2[a]	Complex	High	15
	Micro-Electro Mechanical System	Airflow	Up to 0.05	0.05	Complex	High	16
	Fiber Loop Ringdown Technique	Airflow	5.7-311.0	2.9	Simple	Low	This work
Non-Fiber Optics Based	Micro-Electro Mechanical System	Airflow	0 - 45	0.0284 V/(m/s)[b]	Complex	High	29
	Vibration Amplitude Measurement Method	Airflow	5 - 16	13.2 Ω/(m/s)[b]	Complex	High	30
	Micro-Machined Piezo-Resistivity	Airflow	0 – 25	66 Ω/(m/s)[b]	Simple	Low	31

a) Estimated by the low end of the sensing dynamic ranged examined.
b) Not used for comparison because of different units.
c) All FBG-based sensors are rated as high cost, since an expensive detector (optical spectral analyzer or interrogator) is needed.

2.7 Conclusions

Novel FLRD airflow sensors have been explored to sense high AF based on the micro-bending on the SH. The sensor heads in two different configurations were demonstrated. The performance of both configurations (e.g. horizontal and vertical) was

reproducible and consistent. As compared with other fiber optic airflow sensors, the dynamic range of the FLRD airflow sensor is larger, e.g. a range between 5 to 22.5 slpm. The corresponding AF velocity was between 5.69 and 311.04 m/s defined from converting the flow rates. This new kind of sensor offers a complimentary characteristic of the larger upper limit to those who have a higher sensitivity, but a lower measuring upper limit. In addition, the new FLRD airflow sensor outperforms its peer fiber optic gas flow sensors by its low cost, simplicity, and capability of multiplexing many sensor units into a gas flow sensor network because of the uniform nature of the FLRD signal.

2.8 References

1. Hartman, H. L., Mutmansky, J. M., Ramani, R. V., & Wang, Y. J. (2012). Mine ventilation and air conditioning. John Wiley & Sons.

2. Karacan, C. Ö., Ruiz, F. A., Cotè, M., & Phipps, S. (2011). Coal mine methane: a review of capture and utilization practices with benefits to mining safety and to greenhouse gas reduction. International Journal of Coal Geology,86(2), 121-156.

3. Grattan, K. T. V., & Sun, T. (2000). Fiber optic sensor technology: an overview.Sensors and Actuators A: Physical, 82(1), 40-61.

4. Li, H. N., Li, D. S., & Song, G. B. (2004). Recent applications of fiber optic sensors to health monitoring in civil engineering. Engineering structures, 26(11), 1647-1657.

5. Wang, C. (2009). Fiber loop ringdown—a time-domain sensing technique for multi-function fiber optic sensor platforms: current status and design perspectives. Sensors, 9(10), 7595-7621.

6. Wolfbeis, O. S. (2006). Fiber-optic chemical sensors and biosensors. Analytical Chemistry, 78(12), 3859-3874.

7. Dandridge, A., Kirkendall, C. Eds, and López-Higuera, J. M. (2002) Passive fibre optic sensor networks, Handbook of Optical Fibre Sensing Technology, (Wiley, New York), pp 433-48

8. Cashdollar, L. J., & Chen, K. P. (2005). Fiber Bragg grating flow sensors powered by in-fiber light. Sensors Journal, IEEE, 5(6), 1327-1331.

9. Jewart, C., McMillen, B., Cho, S. K., & Chen, K. P. (2006). X-probe flow sensor using self-powered active fiber Bragg gratings. Sensors and Actuators A: Physical, 127(1), 63-68.

10. Gao, S., Zhang, A. P., Tam, H. Y., Cho, L. H., & Lu, C. (2011). All-optical fiber anemometer based on laser heated fiber Bragg gratings. Optics express,19(11), 10124-10130.

11. Dong, X., Zhou, Y., Zhou, W., Cheng, J., & Su, Z. (2012). Compact anemometer using silver-coated fiber Bragg grating. Photonics Journal, IEEE,4(5), 1381-1386.

12. Wang, X., Dong, X., Zhou, Y., Ni, K., Cheng, J., & Chen, Z. (2013). Hot-Wire Anemometer Based on Silver-Coated Fiber Bragg Grating Assisted by No-core Fiber.

13. Liu, Y., Peng, W., Zhang, X., Liang, Y., Gong, Z., & Han, M. (2013). Fiber-optic anemometer based on distributed Bragg reflector fiber laser technology.Photonics Technology Letters, IEEE, 25(13), 1246-1249.

14. Lee, C. L., Hong, W. Y., Hsieh, H. J., & Weng, Z. Y. (2011). Air gap fiber Fabry–Pérot interferometer for highly sensitive micro-airflow sensing. Photonics Technology Letters, IEEE, 23(13), 905-907.

15. Lee, C. L., Lee, C. F., Li, C. M., Chiang, T. C., & Hsiao, Y. L. (2012). Directional anemometer based on an anisotropic flat-clad tapered fiber Michelson interferometer. Applied Physics Letters, 101(2), 023502.

16. Cheri, M. S., Latifi, H., Aghbolagh, F., Naeini, O. R., Taghavi, M., & Ghaderi, M. (2013). Fabrication, characterization, and simulation of a cantilever-based airflow sensor integrated with optical fiber. Applied optics, 52(14), 3420-3427.

17. Waechter, H., Litman, J., Cheung, A. H., Barnes, J. A., & Loock, H. P. (2010). Chemical sensing using fiber cavity ring-down spectroscopy. Sensors, 10(3), 1716-1742.

18. Wang, C. (2014). Fiber Loop Ringdown Sensors and Sensing. In Cavity-Enhanced Spectroscopy and Sensing (pp. 411-461). Springer Berlin Heidelberg.

19. Stewart, G., Atherton, K., Yu, H., & Culshaw, B. (2001). An investigation of an optical fibre amplifier loop for intra-cavity and ring-down cavity loss measurements. Measurement Science and Technology, 12(7), 843.

20. Brown, R. S., Kozin, I., Tong, Z., Oleschuk, R. D., & Loock, H. P. (2002). Fiber-loop ring-down spectroscopy. The Journal of chemical physics, 117(23), 10444-10447.

21. Wang, C., & Scherrer, S. T. (2004). Fiber ringdown pressure sensors. Optics letters, 29(4), 352-354.

22. Wang, C., & Scherrer, S. T. (2004). Fiber loop ringdown for physical sensor development: pressure sensor. Applied optics, 43(35), 6458-6464.

23. Wang, C., & Herath, C. (2010). High-sensitivity fiber-loop ringdown evanescent-field index sensors using single-mode fiber. Optics letters, 35(10), 1629-1631.

24. Herath, C., Wang, C., Kaya, M., & Chevalier, D. (2011). Fiber loop ringdown DNA and bacteria sensors. Journal of biomedical optics, 16(5), 050501-050501.

25. Kaya, M., Sahay, P., & Wang, C. (2013). Reproducibly reversible fiber loop ringdown water sensor embedded in concrete and grout for water monitoring.Sensors and Actuators B: Chemical, 176, 803-810.

26. Wang, C., & Herath, C. (2010). Fabrication and characterization of fiber loop ringdown evanescent field sensors. *Measurement Science and Technology*,*21*(8), 085205.

27. Sahay, P., Kaya, M., & Wang, C. (2012). Fiber Loop Ringdown Sensor for Potential Real-Time Monitoring of Cracks in Concrete Structures: An Exploratory Study. *Sensors*, *13*(1), 39-57.

28. Von Lerber, T., & Sigrist, M. W. (2002). Cavity-ring-down principle for fiber-optic resonators: experimental realization of bending loss and evanescent-field sensing. *Applied optics*, *41*(18), 3567-3575.

29. Wang, Y. H., Lee, C. Y., & Chiang, C. M. (2007). A MEMS-based air flow sensor with a free-standing micro-cantilever structure. *Sensors*, *7*(10), 2389-2401.

30. Song, C., Aiyar, A. R., Kim, S. H., & Allen, M. G. (2011). Exploitation of aeroelastic effects for drift reduction, in an all-polymer air flow sensor. *Sensors and Actuators A: Physical*, *165*(1), 66-72.

31. Aiyar, A. R., Song, C., Kim, S. H., & Allen, M. G. (2009, January). An All Polymer Air-Flow Sensor Array Using a Piezoresistive Composite Elastomer. In*Micro Electro Mechanical Systems, 2009. MEMS 2009. IEEE 22nd International Conference on* (pp. 447-450). IEEE.

CHAPTER III

FIBER LOOP RINGDOWN HUMIDITY SENSORS

A novel optical fiber relative humidity (RH) sensor based on the evanescent field-fiber loop ringdown (EF-FLRD) technique is demonstrated. The FLRD is a time domain-sensing technique that has been applied to sense versatile applications, such as chemical, physical, and biomedical. A plastic jacket was removed from a section of a single mode fiber (SMF) and followed by a chemical etching process. The sensor was placed inside a chamber, which provides a humidity reference and contains a humidity meter. The presence of moisture in the chamber changes the refractive index of the medium; thus the ringdown time changes due to a change in EF scattering loss induced in the sensor head (SH). The sensor demonstrated a fast response (~ 1 sec), high sensitivity, and excellent reproducibility and reversibly. The EF-FLRD has the capability to measure RH in a wide dynamic range of 4 to 100 % at a constant temperature 20 $\pm$ 1 °C.

3.1 Introduction

Humidity is an important parameter that has to be measured and controlled in many industrial processes and environments, such as food processing and storage, automotive, medical and health, building and construction, meteorological, mineral processing, agriculture, ecology, semiconductor, *etc.* [1-4]. Humidity refers to the content of water vapor in gases. Various terms are associated with humidity, such as absolute

humidity and relative humidity. The absolute humidity indicates the density of water vapor that is the mass of water vapor per unit volume of gas. This measurement is similar to that of atmospheric pressure, thus the absolute humidity is usually not utilized. The most commonly term used for humidity measurement is relative humidity. The more common units used for humidity measurements are relative humidity (RH), parts per million (ppm) of moisture, and dew/frost point (D/FPT) [5].

The relative humidity (RH) is the ratio of the actual vapor pressure in the atmosphere at a specific temperature to the saturation vapor pressure at the same temperature, as given by

$$RH = \frac{P_w}{P_{ws}} \times 100\ \% \tag{3.1}$$

where P_w is the partial pressure of water vapor and P_{ws} is the saturated water vapor pressure at a known temperature, which is often expressed as percentage. In many fields, RH is an important parameter that is used as a monitoring and control tool. For example, for structural health monitoring applications, such as for bridges, buildings, and roadways, the steel reinforcement bars is one of the essentials for strengthens concrete, but the bars are usually inherently covered against corrosion. One of the factors that can create corrosion is a chloride ion that occurs inside a reinforced concrete structure. The occurrence of chlorides in the concrete most usually is from the utilization of salt to melt snow and ice on bridges and roads through winter seasons, especially in these regions that have freezing temperature conditions [6]. While for food process and storage applications, the loss of moisture because of storage and transportation usually limits the shelf life of vegetables and fruit. For example, fruit, such as bell peppers (sweet pepper),

are usually placed in pasteboard boxes and are stored at a RH lower than 90% [7]. In medical application, people with hearing capability loss who have difficulty speaking need a device to help them communicate with other people. Therefore, Morisawa *et al*. [8] evolved a language recognition device based on the moisture contained in breaths as a manner for communication assistance to person with speaking difficulty. During the moisture pattern created in pronunciation, the device had a recognition success of 93%. It was suggested that by employing a fiber optic moisture sensor, a response was shown that the moisture dispersal pattern distinguishing of a breath associated with each vowel might be achieved. Monitoring and measuring humidity is significant importance in such cases.

In recent years, several techniques based on fiber optic sensors have been reported to monitor humidity, which can be categorized as fiber grating, interferometric technique, hybrid approaches, absorption technique, and evanescent wave technique. Humidity sensors based on an optical fiber have been widely studied due to their own advantages, such as immunity to electromagnetic interference, low cost, light weight, miniature size, *etc*. [9-13]. Each of these sensors have their own characteristics through several key parameters, such as sensitivity, response time, objective humidity range, reproducibility, complexity, cost, etc. Fiber grating sensors, including fiber Bragg grating (FBG), short period, or long period grating (LPG), can be created by modulating the refractive index of the fiber core either by subjecting the photosensitive core to intense irradiation or by physical distortion [14-16]. A FBG sensor is convenient for localized sensing and includes complex instrumentation; however, a FBG sensor is affected by temperature fluctuations. The LPG sensors have higher sensitivity to environmental parameters (i.e.,

strain, temperature) than FBG sensors [17]. For instance, relative humidity (RH) sensor based on resistive plate counters (RPC) detector was monitored via a FBG [18]. A commercial polyimide recoated FBG sensor was placed in a box provided with a humidity reference. The wavelength of the Bragg peak was shifted with any change of RH values. As result, the sensor was able to detect RH in a range of 25 % to 65 % in about 10 min. Other groups investigated RH based on long-period grating (LPG) sensor [19]. A tailored layered polyimide coating was deposited on the grating section followed by a silver mirror coated on the end of the fiber. The coated region swelled when the RH increased; thus the refractive index was changed and the resonance wavelength was shifted. In terms of reflective index, the reflective index of the coating layer was decreased due to moisture absorption when the RH was increased. Each RH value kept stabilizing for one hour. The LPG sensor was able to measure RH in a range of 20 % to 80 % at constant temperature of 60 °C.

Interferometric sensors based on optical fibers utilize the interference between two rays, which are propagated through various optical tracks of two fibers or a single fiber. The measurement can be monitored terms of polarization, intensity, wavelength, phase, etc. Different interferometer structure can be fabricated for sensing purposes, such as Michelson, Fabry-Perot, and Mach-Zehnder [20-23]. For example, Shao *et al*. developed an in-fiber Mach-Zehnder interferometer based on a taper fiber for sensing humidity [24]. The interferometer contained two arc-induced ellipsoid fiber tapers and a part of a single mode fiber. A saturated salt solution was used as moisture in a closed vessel. When the fiber tapers were fabricated, the length and the diameter of the taper affected the interferometer. A thin layer of moisture film from water vapor was placed on

the surface of the fiber, which led to the application of a force on the sensor with different RH levels. Thus, the phase difference, the shape, and intensity of the MZI spectrum changed. A certain peak or dip of the spectrum was detected to determined RH. The experimental was effected by temperature, which led to a reduction in RH when temperature was increased. The RH sensor sensed from 50 % to 90 % at a temperature range from 27 °C to 120 °C. Arregui *et al*. reported an optical fiber humidity sensor based on a nano Fabry-Perot cavity [25]. The sensor was fabricated by the self-assembly monolayer technique, followed by a gold colloid coating. The basic idea of the Fabry-Perot optical fiber was based on a varying length of the cavity. A phase was shifted; thus the intensity of the reflection optical power was changed. When the RH was changed, the reflection optical power had a large fringe slope amplitude. The sensor was able to detect RH in a range of 11.3 % to 100 % at constant temperature of 20 °C with a response time less than 1.5 sec.

The evanescent field around the cladding area of a fiber optic can be used to measure different kinds of density modulated fiber optic sensors. Therefore, evanescent wave absorption is created by physically modifying the fiber optic, including etching or removing the cladding layer. This signal is generated by bending the sensor head or a taper of the fiber optic to let the evanescent waves interact with the aim of investigating the associated properly. For example, Alvarez *et al*. used a SMF to measure lower RH based on a wavelength resonance shift technique [26]. The evanescent field was created from a single mode fiber, which was coupled to a TiO_2 waveguide overlay. The transmission response was shown by sharp resonances, which shifted the central wavelength with changing RH. The sensor response was in a range of 0 % to 15 % at a

temperature of 26.1 °C ± 0.6 °C. Another plastic optical fiber RH sensor based on evanescent wave absorption spectroscopy was investigated by Singh and co-workers [27]. A thin polymer film consisting of polyvinyl alcohol and $CoCl_2$ was deposited on a single U-bend plastic-clad silica fiber. In the bending region, the peak intensity of the light was shifted when the sensor absorbed the RH. Different thicknesses and core diameters were tested. The sensor's sensitivity was increased with a smaller diameter and thickness. The time response of the sensor was less than 1 sec with a range from ~ 10 % to more than 90 %.

In this chapter, the evanescent field-fiber loop ringdown (EF-FLRD) technique was employed to monitor the relative humidity over a large dynamic range. The FLRD is a time-domain sensing technique, which was originally from the well-known cavity ringdown spectroscopy (CRDS) technique [e.g., 28-30]. In EF-FLRD, the light is coupled inside a fiber loop, and it travels round the loop for many trips. After each trip, the light intensity is attenuated due to the scattering loss and/or absorption in the fiber loop (sensor head) [31-32]. The EF scattering loss is mainly generated from a different refractive index for a given unit. The sensing mechanism of the EF induces optical losses at the SH. Thus, the ringdown time (sensing signal) changes due to different optical losses, which are associated with a sensing event that occurs in the SH. The sensing signal (ringdown time) is affected by the length of the fiber loop and the total optical loss of the light pulse inside the fiber loop. This can be up to 10 ms or hundreds of μs [29].

A relative humidity (RH) sensor based on EF-FLRD was investigated for the first time. The RH is the ratio of the water vapor in the atmosphere to the saturation value and is often expressed as percentage. The EF-FLRD relative humidity sensor not only has the

general features of fiber optics, such as low cost, light weight, and small size, but also has further advantages, including fast response, no coating needed, simple structure, and independence of temperature. The RH sensor was fabricated by removing the plastic jacket from a small part of a single mode fiber (SMF), followed by 48% hydrofluoric acid (HF) for the etching process. The sensor was placed inside a chamber that provided a humidity reference and contained a humidity meter. Different RH values were tested at a constant temperature of 20 $\pm$ 1 °C. As result, the EF-FLRD sensor has the ability to measure the RH in a wide dynamic range from 4 % to 100 % with excellent reproducibly and fast response.

3.2 Experimental Setup

3.2.1 FLRD System and Fabrication of the SHs

The schematic of the FLRD technique is shown in Figure 3.1 The FLRD technique is divided into two main parts: a sensor control unit and a sensor unit. The sensor control unit consists a photodiode detector (Thorlabs, PDA50B, Newton, NJ, USA), a continuous wave (cw) diode laser (NTT Electronics), and laser control devices, such as a current driver and a temperature control unit. The sensor unit contains a single mode fiber (SMF) loop (SMF 28, Corning, Inc) that is connected to two identical 2 × 1 fiber couplers (Opneti Communication Co., Hong Kong). A small section, *i.e.,* 12 to 20 cm, in the middle of fused silica SMF was spliced to fabricate the sensor head. The connection and disconnection of the sensor from the control system was controlled by two single mode fiber FC/APC connectors. The wavelength of the diode laser was 1515.25 nm.

The cladding and core diameter of the optical fiber were 125 μm and~8.2 μm, respectively. The total optical fiber loop length was 120 m. At the two-leg end, the two identical 2 × 1 fiber couplers were constructed with a split ratio of 0.1:99.9. In the optical fiber loop, the total optical losses of the light included the fiber connectors' insertion losses, absorption losses, and fiber coupler's losses. For each fiber loop round trip, the total optical losses were estimated to be <0.45 dB. The sensor splicing loss was estimated by the fiber splicer (Fusion Splicer, PRO 730) within a typical value of 0.02 to 0.04 dB. After a light beam was coupled into the fiber loop, a ringdown signal was observed by the photodiode detector, which used the signal to feed into a pulse generator (SRS, DG 535) to create a series of the negative square waves. These pulsed square waves were sent to the current driver to decrease the laser current to zero speedily; thus a series of the laser pulses were created by the continuous wave diode laser. The photodiode detector observed a series of pulsed spikes for each laser pulse. These series of spikes created an envelope with an exponential decay. This decay is called the ringdown time curve, which is the FLRD technique sensing signal.

The sensor fabrication was described in previous publications [33,34]. After the plastic jacket was removed from a section of the SMF with a chosen length, i.e., 12-20 cm, the section was completely immersed into a 48% hydrofluoric acid (HF) solution for the etching process for proximately 34 min. Figure 3.1 (a) and (b) demonstrates the part of SMF to be etched that serves as SH and the etched fiber SH, respectively. During the etching process, the ringdown was continuously monitored [33].

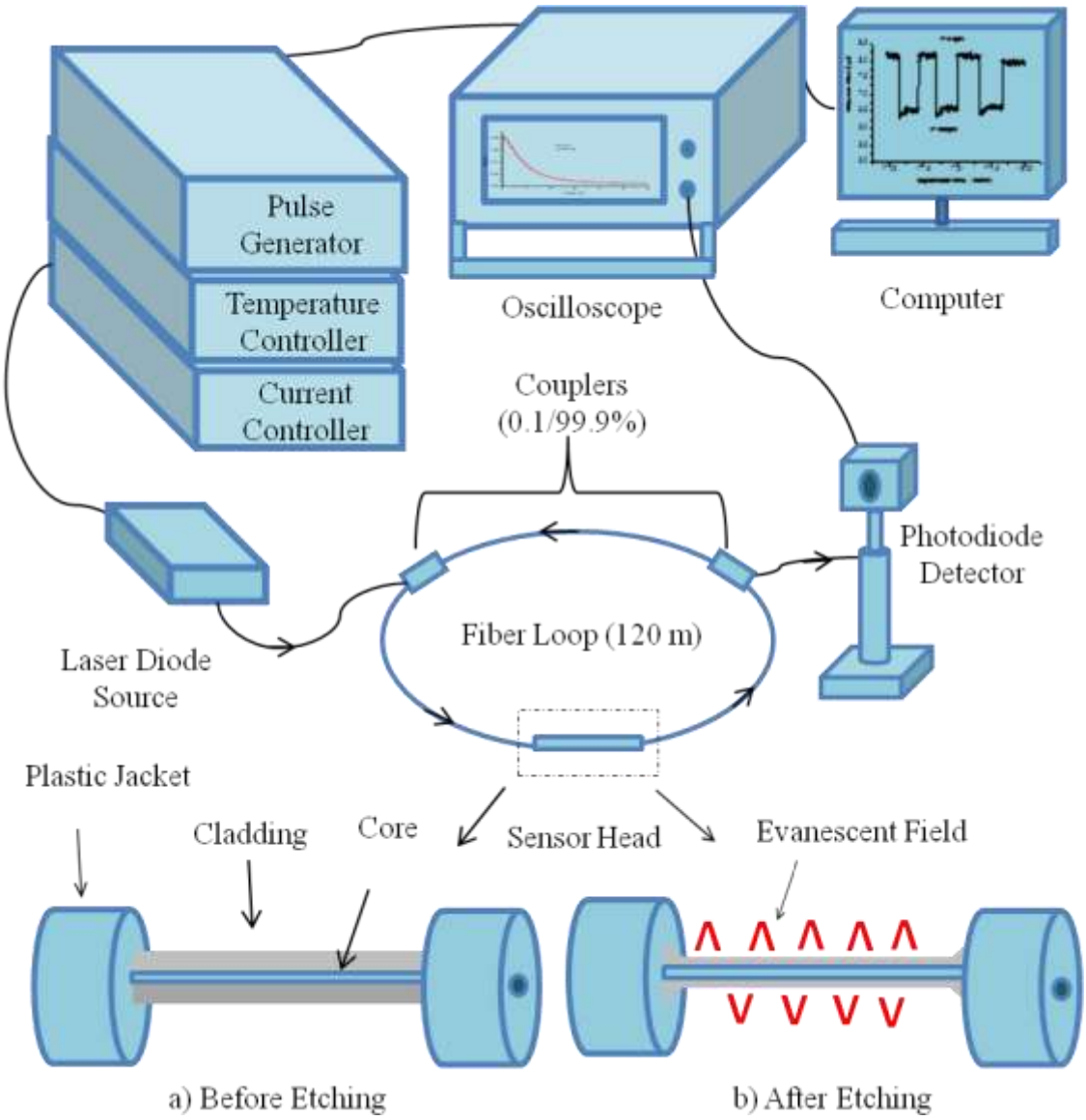

Figure 3.1 The schematic of the fiber loop ringdown (FLRD) technique.

The light beam is transferred through the second coupler and collected via the photodiode detector and the detected signal is transferred to the oscilloscope to detect the ringdown curve. (a). The sensor head is shown before etching with 48% HF solution. (b). The sensor head is shown after etching with 48% HF solution. The evanescent field is shown in the surrounding surface of the sensor head by a small spike, which occurs on the surface of the sensor head that is between the core and the external medium.

3.2.2 The Chamber of the Relative Humidity Sensor

The sensor was placed in a sealed chamber provided with inlet and outlet setting on opposite sides to allow gas to flow, as shown in Figure 3.2. Nitrogen (N_2) gas was flowed inside the chamber to dry the air. Also, an airflow source was flowed inside two bottles connected to each other, as seen in Figure 3.2. One contained water (warm/hot) to obtain different moisture levels inside the chamber. Another bottle was used to collect any water drops that were coming from the first bottle. There was a switch key to alternate between the airflow source and N_2 gas. A commercial meter (Rotronic, HygroPalm, HP 21) was used to monitor temperature and RH with a specified accuracy at 23 °C ± 5 °C of 1 % RH and ± 0.2 °C. The temperature was constant at 20 ± 1 °C, and the RH inside the chamber was cycled from 4 to 100 %.

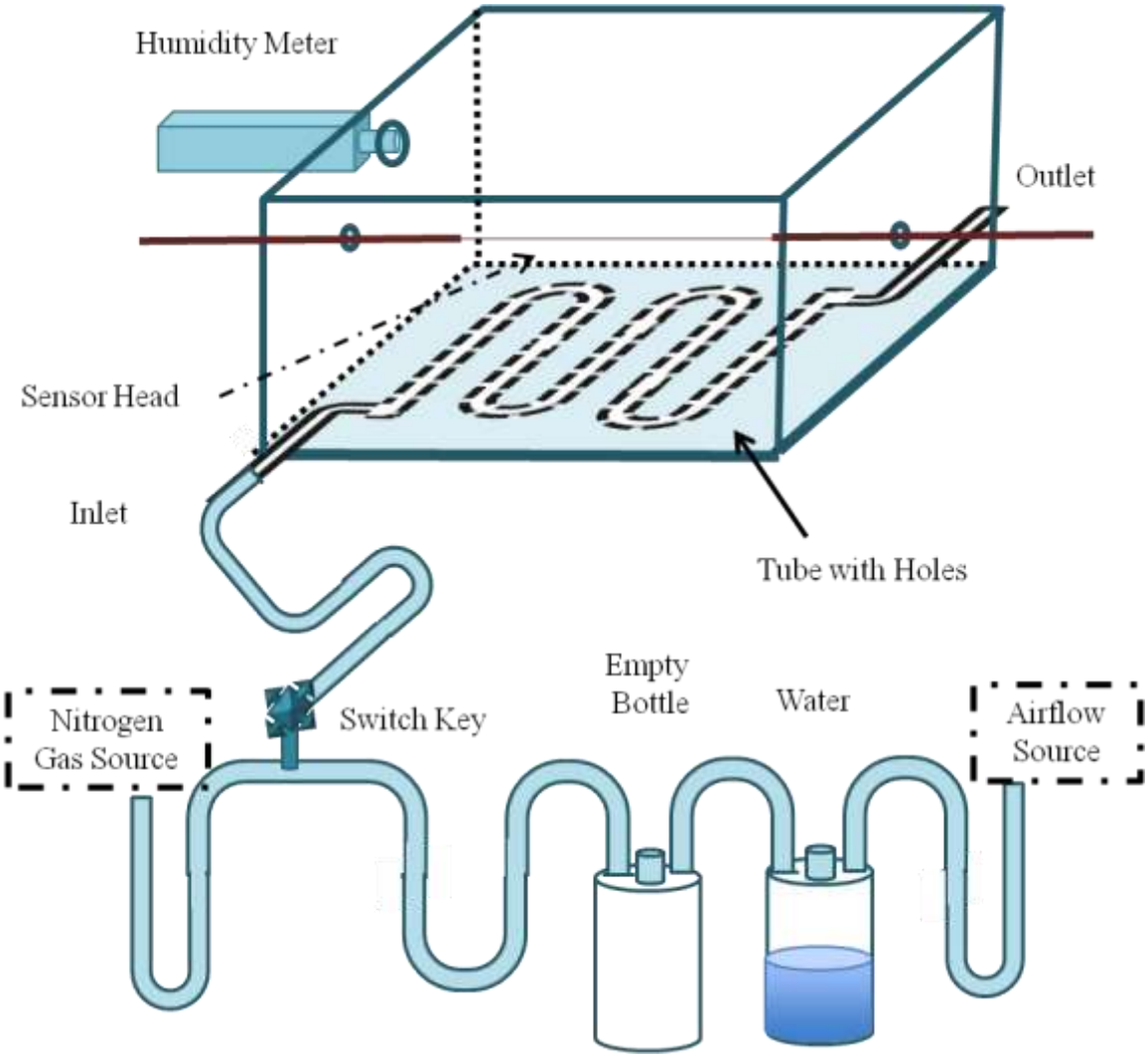

Figure 3.2 The FLRD chamber for monitoring relative humidity.

3.3 Principle of the EF-FLRD Humidity Sensors

A light pulse is coupled into a fiber loop and travels inside the fiber loop for many round trips. During each round trip, the intensity of the light pulse was decreased because of the internal optical loss [11]. After each round trip, different intensities of the transmitted light were observed by the photodiode detector. Therefore, the change of the light intensity, which is observed by the photodiode detector, can be given as

$$\frac{dI}{dt} = -\frac{IAc}{nL} \tag{3.2}$$

where I is the light pulse intensity at time t (when the light pulse is coupled into the fiber loop and shuts down, the time is zero), c is the speed of the light in vacuum, L is the length of the fiber loop, n is the fiber loop reflective index, and A is the total transmission loss of the fiber loop of the light pulse for each round trip. Solution of Equation (3.1) demonstrates the temporal behavior of the light intensity I detected by the detector and is expressed in Equation (3.3)

$$I = I_0\, e^{-\frac{c}{nL}At} \tag{3.3}$$

The necessary time for the light intensity I to decrease to $1/e$ of the original light intensity, I_0, in the absence of any humidity is denoted as the ringdown time, τ_0, and is given by Equation (3.4)

$$\tau_{0=\frac{nL}{cA}} \tag{3.4}$$

$$\tau = \frac{nL}{c(A+B)} \tag{3.5}$$

The total transmission loss A for a given FLRD sensor can be defined by the physical parameters of the sensor unit, including the reflective index, the fiber absorption loss, the couplers' insertion loss, and the fiber loop length. For a given fiber loop, the total transmission losses remains constant. When an external action, such as absorption or change in any measurement, including stress, pressure, temperature, etc., happens in the sensing region of the fiber loop (sensor head), the result is an additional optical loss B of the light in the fiber loop. This causes a change in ringdown time (sensing signal), τ, and is shown in Equation (3.5). From Eq.(3.4) and (3.5), we can obtain

$$B = \frac{nL}{c}\left(\frac{1}{\tau} - \frac{1}{\tau_0}\right) \quad (3.6)$$

The principle of the EF-ERLD is shown in Equation (3.6), in which the additional optical loss, B, is defined by measuring the ringdown time with activity τ and without any sensing activity τ_0. In this work, the FLRD technique was explored to detect relative humidity based on the evanescent field-fiber loop ringdown (EF-FLRD) technique. The difference of the optical loss, B, of the light beam in the fiber loop is between the presence of moisture and no moisture inside the chamber. Different moisture levels (RH) present in the chamber affected the reflective index of the air. Thus, the EF scattering loss changes because of the change in index of refraction [31,33].

3.4 Results and Discussion

Figures 3.3 to 3.5 show the typical response of the EF-FLRD sensor for monitoring relative humidity. Different RH values were tested at a constant temperature of $20 \pm 1\ ^{\circ}C$. In Figure 3.3, the first part of experiment included flowing the N_2 gas to get dry air. The N_2 gas was kept flowing for a few minutes and the ringdown time was recorded. Then, the N_2 gas was switched off and the airflow was turned on inside a bottle of warm water to increase the moisture level inside the chamber and also kept flowing for a few minutes to record the ringdown time. The RH in Figure (3.3) was in a range from 54 to 23.6 % at a constant temperature of 20 ± 1 °C. When the moisture (wet air) was presented in the chamber, the ringdown time increased because the refractive index of the higher RH (wet air) was higher than the refractive index of the lower RH (dry air). The vertical drop line occurred when the N_2 gas only was flowed. Therefore, the ringdown time sharply decreased due to no moisture around the sensor head. From points A - C,

after the N_2 gas was turned on, the moisture level inside the chamber gradually decreased until it reached the RH level target, as shown in Figure (3.3). Hence, the ringdown time started to decrease due to no moisture around the sensor. From point D to F, when the switch key was turned on to the airflow source, the moisture level gradually increased until it stabilized at the specific RH level; thus the ringdown time increased. The ringdown times of RH of 54 % and 23.6 % were 6.5 µs and 5.9 µs, respectively. In order to test the reproducibility of the sensor, the switch key was used to alternate between the airflow and N_2 gas for increasing or decreasing the moisture inside the chamber, respectively.

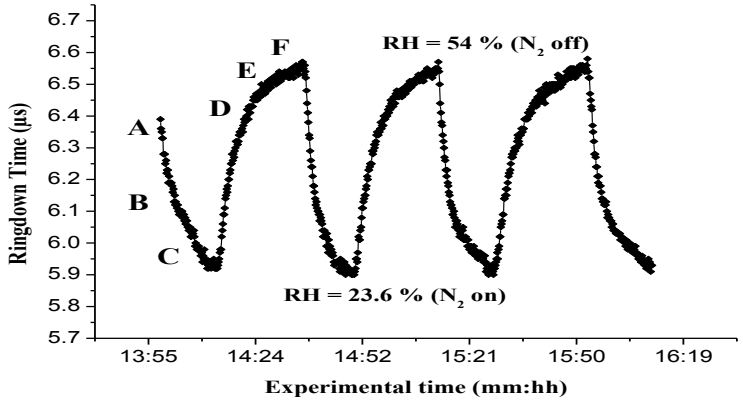

Figure 3.3 Response of the FLRD relative humidity sensors in a range of 54 % to 23.6 %.

In order to have slight variations of RH, the chamber was not perfectly sealed. In Figure 3.4, the chamber's cover was opened to the room to measure the RH of the room. Then, N_2 gas was flowed to get lower moisture around the sensor. The sensor was able to detect a RH range of 59 % to 36 %, and the ringdown times were 6.3 µs and 6.7 µs,

respectively. The reversible response of the EF-FLRD relative humidity sensor was verified by alternately cycling between 59 % and 36 %.

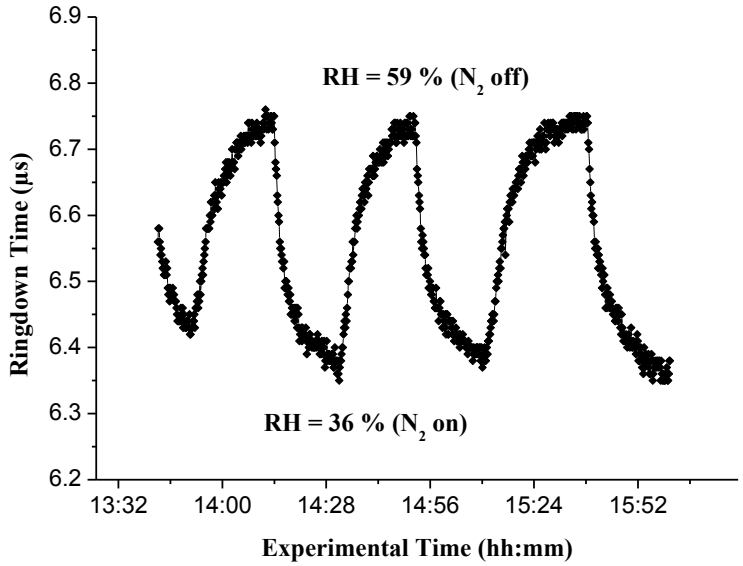

Figure 3.4 Response of the FLRD sensor to the room relative humidity.

In Figure 3.5 (a-e), the data was obtained by the same procedures using hot water inside the first bottle to get higher RH levels. The time response to switch between high humidity to low humidity was between ~ 15 sec to ~3 min, depending on the moisture variation inside the chamber. For example, the higher moisture inside the chamber needed a longer time to reduce the moisture to a lower level.

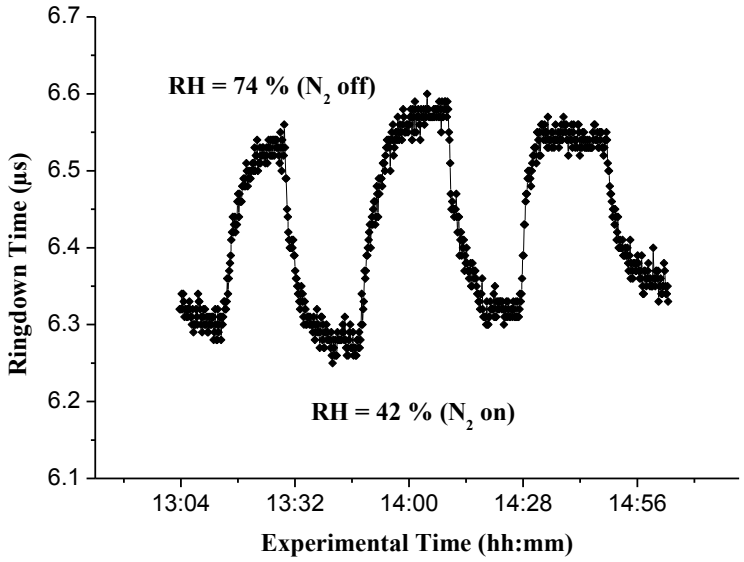

(a)

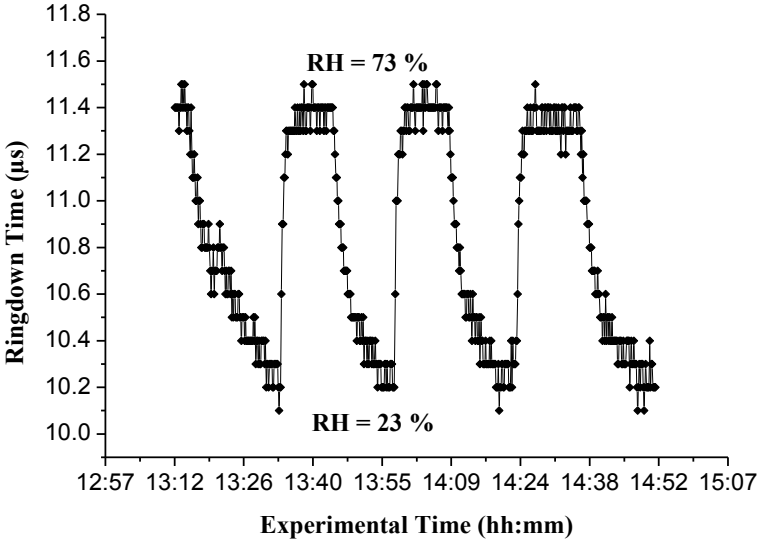

(b)

Figure 3.5 (a-e) Response of the FLRD relative humidity sensor for different ranges.

(a) RH = 42- 74 % (b) RH = 23 -73 % (c) RH = 49 -94 % (d) RH = 4-85 % (e) RH = 49 – 100 %

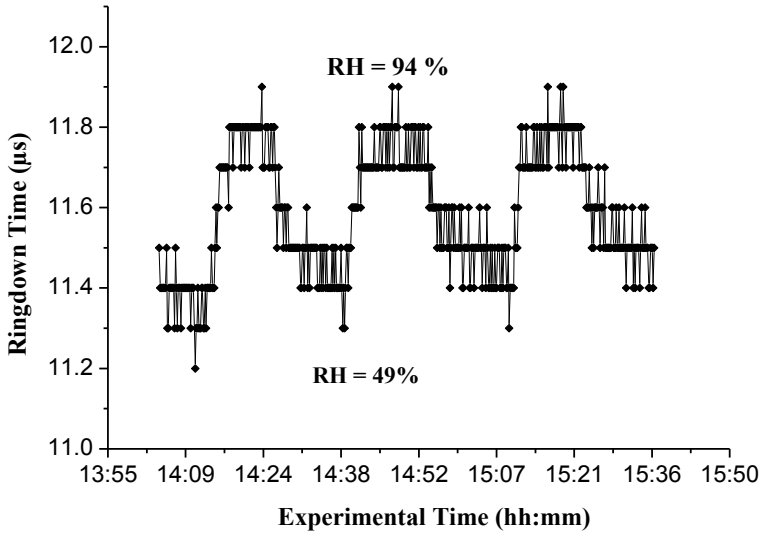

(c)

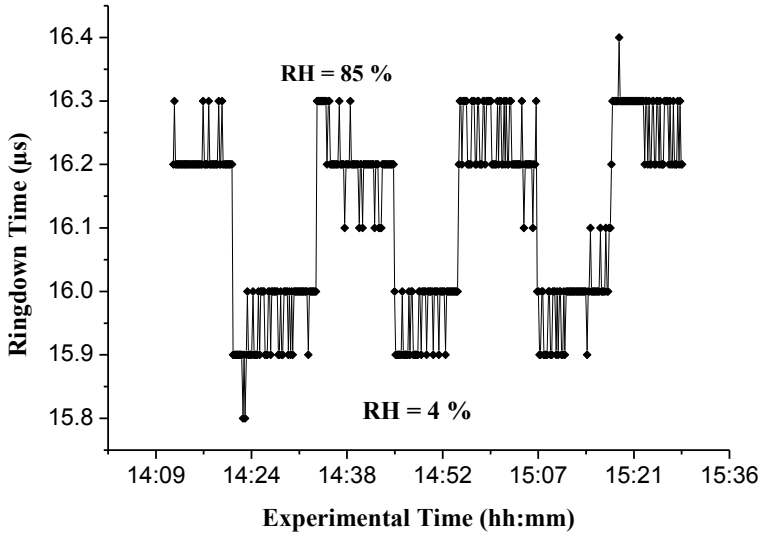

(d)

Figure 3.5 (continued)

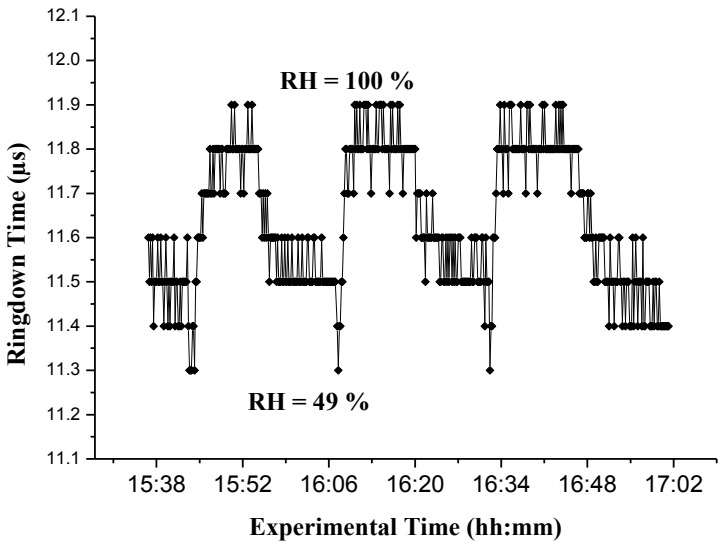

(e)

Figure 3.5 (continued)

In this work, different sensors were used to monitor RH, and each of these sensors had different sensitivities due to the sensor head fabrication processes and sensor fiber loops. There are some factors that can affect the sensors' sensitivity, such as the length of the fiber loops, the length of the sensor head, and the total optical loss A. More details about sensor fabrication and their sensitivity can be seen in [33]. Even with different sensor sensitivity, the ringdown time was still higher at high RH levels due to the moisture around the sensor head and lower when the RH level was low.

3.5 Detection Sensitivity

The minimum sensitivity of the EF-FLRD to detectable relative humidity (%) was investigated. The relative humidity sensor baseline stability was determined as σ_τ / τ where σ_τ is one standard deviation of the ringdown time and τ is the average of the ringdown times. The FLRD relative humidity sensors had a baseline stability of 0.2 % by

averaging over 100 ringdown events. The data in Figure (3.3) was used as an example to calculate the minimum detection of the RH (%). The difference of the ringdown time was 0.6 μs for the RH range from 54 % to 23. %. The ringdown time with respect to the 0.2% baseline noise was from the ringdown time 5.9 μs is 0.012 μs. Thus, a theoretical detection sensitivity limit of the RH sensor is approximately 1 %

3.6 Comparison of the EF-FLRD Relative Humidity Sensors with Other Works Based on Fiber Optic Sensor

There are several humidity sensors based on different types of optical fibers, such as fiber Bragg gratings (FBG) [35], tilted fiber Bragg gratings (TFBG) [36], single mode fiber (SMF) [37], plastic optical fiber [38], long period fiber gratings (LPG) [39], hybrid fiber gratings [40], photonic crystal fiber (PCF) structures [41], etc. Each of these sensors have their own technique, materials, limitations, etc.

For example, Correia *et al*. used the sol-gel method to coat a FBG relative humidity sensor with an organo-silica hybrid material [35]. The sensor was tested inside concrete blocks. The Bragg wavelength was changed when the FBG sensor swelled due to RH. The time response was 8.1 ± 1.1 min and 16.4 ± 0.4 min for different FBG coatings. The sensor was able to measure RH in a range from 15 % to 95 %. Kronenberg *et al*. investigated a FBG relative humidity sensor with different coating thicknesses [42]. The sensor's sensitivity increased with higher thicknesses. When the RH was increased further, the Bragg wavelength shifted to higher values. The sensor measured the RH and temperature in ranges from 10 % to 90% and from 13°C to 60 °C, respectively. David *et al*. described a polymer-coated FBG sensor to detect RH [43]. The sensitivity and the time response of the sensor were affected by coating thickness and fiber diameter. The

coating thickness (e.g., 4 μm and ~ 2 μm) needed about 5 sec and a shorter time, respectively, to detect RH. When the sensor was etched using 48% hydrofluoric acid to reduce the diameter, the sensitivity was improved to detect wider a range of ~ 15 % to 95 %. Another group reported a sub wavelength diameter tapped optical fiber to monitor RH [44]. The subwavelength diameter fiber was fabricated by using a flame taper-drawing technique followed by a gelatin film coating. The sensor was placed in a chamber provided with a gas flow system. The taper sensor detected the RH ranging from 9% to 94% in about 70 ms. Otsuki *et al*. reported lower RH levels down to 0 based on an open air-gap configuration [45]. A polymer-clad silica fiber sensor was coated with a film containing of Rhodamine B-doped hydroxypropyl cellulose. The transmitted light changed when the RH increased. The sensor was able to measure RH in a range of 0 to 95% with a response time of ~ 2 min. Kharaz *et al*. investigated a multi-point distributed humidity sensor via a multimode optical fiber based on the absorption spectrum of a colorimetric reagent (cobalt chloride) [46]. A thin gelatin film was deposited on the surface of the sensor. The spectral absorption wavelength of the sensor was affected by the change RH values. The sensor monitored the RH in a range of 20 to 80 % and a temperature range of 25 to 50 °C with a time constant of 1 sec. Li *et al.* used a photonic crystal fiber interferometer (PCFI) to measure RH [47]. A sensor was formed by fusion splicing; a short length of PCFI was between two single mode fibers, containing air holes of the PCFI in the splicing regions which fully collapsed. A dip-coating technique was used to coat a layer of polyvinyl alcohol on the sensor. The transmission spectrum was shifted when humidity increased. The sensor was able to detect RH in a range of 20 to 95 % at a constant temperature of 25 °C. Wu *et al.* investigated a RH sensor based on a

small-core SMF [48]. Different thicknesses of a thin film of polyethylene oxide (PEO) were deposited on the surface of the sensor via a motor controlled translation stage. The PEO coating affected the sensor sensitivity; the larger thicknesses had higher sensitivity compared to lower thicknesses. The sensor's response was due to a decrease in the refractive index of the PEO when the RH increased. The wavelength decreased when RH increased. The sensor was able to detect RH in a range from 80% to 83% for 430 nm per RH unit and 83% to 95% for 50 nm per RH unit at a temperature of 19.2 $\pm$ 0.5 °C. Mathew *et al*. investigated a RH sensor based on a bent SMF [49]. The sensor was coated by Agarose and placed inside a chamber; the sensitivity of the sensor depended on the observed longer wavelengths. An RH increased the insertion loss variation and the wavelength. The sensor was able to measure from 25 to 90 % with a time response of 50 ms. Table 3.1 illustrates different RH sensors based on their sensing technique, dynamic range, temperature range, time response, and coating material.

In the comparison, the EF-FLRD technique has wider ranges than other techniques. As shown in the table, most of the techniques needed to coat the sensor using different material while EF-FLRD sensor did not need to coat. The EF-FLRD sensor was made from one section of partially-etched SMF. Also, EF-FLRD has the ability to measure relative humidity in large dynamic range from 4 to 100 % at a constant temperature of 20 $\pm$ 1 °C. The EF-FLRD response did not depend on any factors, such as temperature, coating thickness, etc. There was no deformation, such as swelling in the EF- FLRD sensor. Moreover, the EF-FLRD sensor was easy to fabricate and is not costly. There were no complex instruments needed to use it. The time response to switch from lower humidity to higher humidity was between 15 sec and $\sim$ 3 min, depending on

the RH variation while the sensor response to RH was ~ 1 sec. As a result, all these features make the EF-ELRD technique unique and attractive for other applications.

Table 3.1 Summary of relative humidity sensors that are based on different types of fiber optics sensors.

Fiber Optics Sensors Type	Sensing Technique	Dynamic Range (%RH)	Temperature (C°)	Response Time	Coating Material	Ref
FBG	Strain induced Bragg wavelength	5 - 95	-	-	Organo-silica hybrid	35
	Thin-core fiber modal interferometer	20 - 90	-	2 - 10 sec	Poly (N-ethyl-4-vinylpyridinium chloride) (P4VP·HCl) and poly (vinylsulfonic acid, sodium salt) (PVS)	50
Optical Fiber	Localized surface plasmon resonance and Lossy-mode resonance	20 - 70	25	2 hr	Nanoparticles (NG NPs)	51
Plastic Optical Fiber	Ray tracing method	20 - 80	-	-	hydroxyethylcellulose and polymethylmethacrylate	38
PCF	Photonic crystal fiber interferometer	40 - 90	24 ± 1	75 ms	Agarose film	41
Photonic bandgap fiber	Wavelength modulation spectroscopy technique	0 – 95	-	-	No coating	52
SMF	Telecommunications wavelength	> 62% > 80%	~ 22 – 24	-	Gelatin and polyethylene oxide films	37
TFBG	Intensity variation measurement	20 - 74	-	< 2 sec	Polyvinyl alcohol	36
LPG	LPG resonance band wavelength shift	33 - 97	-	1 min	Polyvinyl alcohol	39
FBG-PCF	Transmission loss measurement	20 - 90	22	<1 sec	Agarose	40
SMF	Fiber Loop Ringdown	4 - 100	20 ± 1	~ 1 sec	No coating	This work

3.7 Conclusions

A new type of EF-FLRD sensor for relative humidity sensing has been demonstrated. The EF-FLRD principle and configuration has been described. The sensor was fabricated and placed inside the chamber, which provided a humidity reference and meter. The EF-FLRD was able to monitor relative humidity with a larger dynamic range from 4 to 100 % at a constant temperature of 20 $\pm$ 1 °C. Based upon the large dynamic range, the EF-FLRD sensor has further advantages compared to other humidity sensors, such as fast response, good reversibility, no coating need, low cost, and independent of temperature. This new type of the optical fiber humidity sensor has high potential for real time monitoring applications.

3.8 References

1. Yamazoe, N., and Shimizu, Y. (1986). Humidity sensors: principles and applications. *Sensors and Actuators*, *10*(3), 379-398.

2. Yeo, T. L., Sun, T., and Grattan, K. T. V. (2008). Fibre-optic sensor technologies for humidity and moisture measurement. *Sensors and Actuators A: Physical*, *144*(2), 280-295.

3. Alwis, L., Sun, T., and Grattan, K. T. V. (2013). Optical fibre-based sensor technology for humidity and moisture measurement: Review of recent progress. *Measurement*, *46*(10), 4052-4074.

4. Traversa, E. (1995). Ceramic sensors for humidity detection: the state-of-the-art and future developments. *Sensors and Actuators B: Chemical*, 23(2), 135-156.

5. Chen, Z., and Lu, C. (2005). Humidity sensors: a review of materials and mechanisms. *Sensor letters*, *3*(4), 274-295.

6. Lam, C. C. C., Mandamparambil, R., Sun, T., Grattan, K. T., Nanukuttan, S. V., Taylor, S. E., and Basheer, P. M. (2009). Optical fiber refractive index sensor for chloride ion monitoring. *Sensors Journal, IEEE*, *9*(5), 525-532.

7. Dijkink, B. H., Tomassen, M. M., Willemsen, J. H., and van Doorn, W. G. (2004). Humidity control during bell pepper storage, using a hollow fiber membrane contactor system. *Postharvest Biology and Technology*, *32*(3), 311-320.

8. Morisawa, M., Natori, Y., Taki, T., and Muto, S. (2010). Recognition of devoiced vowels using optical microphone made of multiple POF moisture sensors. *Electronics and Communications in Japan*, *93*(9), 12-18.

9. Grattan, K. T. V., and Sun, T. (2000). Fiber optic sensor technology: an overview. *Sensors and Actuators A: Physical*, *82*(1), 40-61.

10. Li, H. N., Li, D. S., and Song, G. B. (2004). Recent applications of fiber optic sensors to health monitoring in civil engineering. *Engineering Structures*, *26*(11), 1647-1657.

11. Wang, C. (2009). Fiber loop ringdown—a time-domain sensing technique for multi-function fiber optic sensor platforms: current status and design perspectives. *Sensors*, *9*(10), 7595-7621.

12. Dandridge, A. and Kirkendall, C. (2002) *Passive fiber optic sensor networks* (pp. 433-448). J. M. López-Higuera (Ed.). John Wiley.

13. Grattan, K. T. V. and Meggitt, B. T. (1998) Optical Fiber Sensor Technology Vol 2: Devices and Technology 2 (Berlin: Springer)

14. Savin, S., Digonnet, M. J. F., Kino, G. S., and Shaw, H. J. (2000). Tunable mechanically induced long-period fiber gratings. *Optics Letters*, *25*(10), 710-712.

15. Wang, L., Lin, C., and Chern, G. (2001). Periodical corrugated structure for forming sampled fiber Bragg grating and long-period fiber grating with tunable coupling strength. *Journal of Lightwave Technology*, *19*(8), 1212-1221. doi:10.1109/50.939803

16. James, S. W., and Tatam, R. P. (2003). Optical fibre long-period grating sensors: Characteristics and application. *Measurement Science and Technology*, *14*(5), R49-R61. doi:10.1088/0957-0233/14/5/201

17. Bhatia, V. (1996). Properties and sensing applications of long-period gratings (Doctoral dissertation), Virginia Polytechnic Institute and State University, Virginia

18. Caponero, M. A., Polimadei, A., Benussi, L., Bianco, S., Colafranceschi, S., Passamonti, L., and Vendittozzi, C. (2013). Monitoring relative humidity in RPC detectors by use of fiber optic sensors. *Journal of Instrumentation*, *8*(03), T03003.

19. Alwis, L., Sun, T., and Grattan, K. V. (2013). Analysis of Polyimide-Coated Optical Fiber Long-Period Grating-Based Relative Humidity Sensor. *IEEE Sensors Journal*, *13*(2), 767-771.

20. Lee, B. H., Kim, Y. H., Park, K. S., Eom, J. B., Kim, M. J., Rho, B. S., and Choi, H. Y. (2012). Interferometric fiber optic sensors. *Sensors*, *12*(3), 2467-2486.

21. Fu, H., Shu, X., Zhang, A., Liu, W., Zhang, L., He, S., and Bennion, I. (2011). Implementation and characterization of liquid-level sensor based on a long-period fiber grating Mach–Zehnder interferometer. *IEEE*, *Sensors Journal,11*(11), 2878-2882.

22. Frazão, O., Marques, L. M., Santos, S., Baptista, J. M., and Santos, J. L. (2006). Simultaneous measurement for strain and temperature based on a long-period grating combined with a high-birefringence fiber loop mirror. *IEEE, Photonics Technology Letters*, *18*(22), 2407-2409.

23. Wang, A., Xiao, H., Wang, J., Wang, Z., Zhao, W., and May, R. G. (2001). Self-calibrated interferometric-intensity-based optical fiber sensors. *Journal of Lightwave Technology*, *19*(10), 1495.

24. Shao, M., Qiao, X., Fu, H., Zhao, N., Liu, Q., and Gao, H. (2013). An in-fiber Mach-Zehnder Interferometer Based on Arc-induced Tapers for High Sensitivity Humidity Sensing.

25. Arregui, F. J., Liu, Y., Matias, I. R., and Claus, R. O. (1999). Optical fiber humidity sensor using a nano Fabry–Perot cavity formed by the ionic self-assembly method. *Sensors and Actuators B: Chemical*, *59*(1), 54-59.

26. Alvarez-Herrero, A., Guerrero, H., and Levy, D. (2004). High-sensitivity sensor of low relative humidity based on overlay on side-polished fibers. *IEEE, Sensors Journal*, *4*(1), 52-56.

27. Khijwania, S. K., Srinivasan, K. L., and Singh, J. P. (2005). An evanescent-wave optical fiber relative humidity sensor with enhanced sensitivity. *Sensors and Actuators B: Chemical*, *104*(2), 217-222.

28. Waechter, H., Litman, J., Cheung, A. H., Barnes, J. A., and Loock, H. P. (2010). Chemical sensing using fiber cavity ring-down spectroscopy. *Sensors*, *10*(3), 1716-1742.

29. Wang, C. (2014). Fiber Loop Ringdown Sensors and Sensing. In *Cavity-Enhanced Spectroscopy and Sensing* (pp. 411-461). Springer Berlin Heidelberg.

30. Brown, R. S., Kozin, I., Tong, Z., Oleschuk, R. D., and Loock, H. P. (2002). Fiber-loop ring-down spectroscopy. *The Journal of Chemical Physics*, *117*(23), 10444-10447.

31. Wang, C., and Herath, C. (2010). High-sensitivity fiber-loop ringdown evanescent-field index sensors using single-mode fiber. *Optics Letters*, *35*(10), 1629-1631.

32. Kaya, M., Sahay, P., & Wang, C. (2013). Reproducibly reversible fiber loop ringdown water sensor embedded in concrete and grout for water monitoring. *Sensors and Actuators B: Chemical*, *176*, 803-810.

33. Wang, C., and Herath, C. (2010). Fabrication and characterization of fiber loop ringdown evanescent field sensors. *Measurement Science and Technology*, *21*(8), 085205.

34. Herath, C., Wang, C., Kaya, M., and Chevalier, D. (2011). Fiber loop ringdown DNA and bacteria sensors. *Journal of Biomedical Optics*, *16*(5), 050501-050501.

35. Correia, S. F., Antunes, P., Pecoraro, E., Lima, P. P., Varum, H., Carlos, L. D., ... and André, P. S. (2012). Optical fiber relative humidity sensor based on a FBG with a Di-ureasil coating. *Sensors*, *12*(7), 8847-8860.

36. Miao, Y., Liu, B., Zhang, H., Li, Y., Zhou, H., Sun, H., and Zhao, Q. (2009). Relative humidity sensor based on tilted fiber Bragg grating with polyvinyl alcohol coating. *IEEE, Photonics Technology Letters*, *21*(7), 441-443.

37. Bownass, D. C., Barton, J. S., and Jones, J. D. C. (1998). Detection of high humidity by optical fibre sensing at telecommunications wavelengths. *Optics Communications*, *146*(1-6), 90-94.

38. Muto, S., Suzuki, O., Amano, T., and Morisawa, M. (2003). A plastic optical fibre sensor for real-time humidity monitoring. *Measurement Science and Technology*, *14*(6), 746.

39. Venugopalan, T., Sun, T., and Grattan, K. T. V. (2008). Long period grating-based humidity sensor for potential structural health monitoring. *Sensors and Actuators A: Physical*, *148*(1), 57-62.

40. Mathew, J. J., Semenova, Y. Y., and Farrell, G. G. (2013). Fiber optic hybrid device for simultaneous measurement of humidity and temperature. *IEEE Sensors Journal*, *13*(5), 1632-1636. doi:10.1109/JSEN.2013.2238229

41. Mathew, J., Semenova, Y., and Farrell, G. (2013). Effect of coating thickness on the sensitivity of a humidity sensor based on an Agarose coated photonic crystal fiber interferometer. *Optics Express*, *21*(5), 6313-6320.

42. Kronenberg, P., Rastogi, P. K., Giaccari, P., and Limberger, H. G. (2002). Relative humidity sensor with optical fiber Bragg gratings. *Optics Letters*, *27*(16), 1385-1387.

43. David, N. A., Wild, P. M., and Djilali, N. (2012). Parametric study of a polymer-coated fibre-optic humidity sensor. *Measurement Science and Technology*, *23*(3), 035103.

44. Zhang, L., Gu, F., Lou, J., Yin, X., and Tong, L. (2008). Fast detection of humidity with a subwavelength-diameter fiber taper coated with gelatin film. *Optics Express*, *16*(17), 13349-13353.

45. Otsuki, S., Adachi, K., and Taguchi, T. (1998). A novel fiber-optic gas sensing arrangement based on an air gap design and an application to optical detection of humidity. *Analytical Sciences*, *14*(3), 633-635.

46. Kharaz, A., and Jones, B. E. (1995). A distributed optical-fibre sensing system for multi-point humidity measurement. *Sensors and Actuators A: Physical*, *47*(1), 491-493.

47. Li, T., Dong, X., Chan, J., Ni, K., Zhang, S., and Shum, P. (2013). Humidity sensor with a PVA-coated photonic crystal fiber interferometer.

48. Wu, Q., Semenova, Y., Mathew, J., Wang, P., and Farrell, G. (2011). Humidity sensor based on a single-mode hetero-core fiber structure. *Optics Letters*, *36*(10), 1752-1754.

49. Mathew, J., Semenova, Y., and Farrell, G. (2012). A fiber bend based humidity sensor with a wide linear range and fast measurement speed. *Sensors and Actuators A: Physical*, *174*, 47-51.

50. Gu, B., Yin, M., Zhang, A. P., Qian, J., & He, S. (2011). Optical fiber relative humidity sensor based on FBG incorporated thin-core fiber modal interferometer. *Optics Express*, *19*(5), 4140-4146.

51. Rivero, P. J., Urrutia, A., Goicoechea, J., and Arregui, F. J. (2012). Optical fiber humidity sensors based on Localized Surface Plasmon Resonance (LSPR) and Lossy-mode-resonance (LMR) in overlays loaded with silver nanoparticles. *Sensors and Actuators B: Chemical*.

52. Mohd Noor, M. Y., Khalili, N., and Peng, G. D. (2013). All-Fiber Optic Humidity Sensor Based on Photonic Bandgap Fiber and Digital WMS Detection.

CHAPTER IV

CONCLUSIONS AND FUTURE WORK

In this thesis, the fiber loop ringdown technique was used to monitor two different physical parameters. Gas flow and humidity sensors were investigated .The gas flow sensor was demonstrated based on the micro-bending sensing mechanism while the humidity sensor monitored by using the evanescent field-fiber loop ringdown technique. The principle and the experimental setup for both sensors were demonstrated. Also, the results and discussion were presented.

4.1 Summary

In Chapter I, fiber optic sensors and their advantages were illustrated. The fiber loop ringdown technique, which evolved from the well-known cavity ringdown spectroscopy technique, was described [1]. The advantages, the principle, and instruments of FLRD were also illustrated [2].

In Chapter II, a gas flow sensor was investigated based on the micro-bending sensing mechanism [3,4]. In this case, the optical losses were induced when the air flowed toward the sensor head; thus physical deformation was created. The sensor head was applied to sense AF at various AF rates. Two different sensor head configurations were demonstrated to monitor different airflow rates. Both configurations gave excellent results, including reproducibility and reversibility. The sensor heads have able to measure

a large dynamic range of 5 to 22.5 slpm, with a theoretical detection sensitivity limit of 0.1 slpm. The corresponding AF speeds were measured in the range of 5.69 m/s to 311.04 m/s. As a result, the sensor verified fast response of less than one second. Furthermore, the sensor's response had excellent reproducibility and reversibility. The sensor's fabrication was simple to fabricate with low cost.

In Chapter III, a relative humidity sensor was described based on the evanescent field-fiber loop ringdown technique [5,6]. The sensor head was fabricated by removing the plastic jacket and followed by using HF acid for etching process. The sensor head was placed inside the chamber provided with a humidity reference and meter. The presence of different moisture levels inside the chamber led to a change in the refractive index of the medium; thus the ringdown time changes due to a change in the evanescent field scattering loss induced in the sensor head. The sensors had a fast response ($\sim$ 1 sec) with excellent reproducibility and reversibility. The EF-FLRD sensor has the capability of measuring RH in a wide dynamic range of 4% to 100 % at a constant temperature of 20 $\pm$ 1 °C.

4.2 Future Applications

In the mining field, ventilation underground is essential to miners. In some strategic positions, the airflow attenuates because of an increase in gas emission rates that lead to the creation of a combustible gas mixture [7,8]. Therefore, applying the airflow-fiber loop ringdown sensors under the ground to monitor airflow gives two warnings. First, it protects miners from the weakness or failure of ventilation. Second, it gives early warning to miners. In addition, for industrial gases, a gas flow sensor is needed to monitor any leaking gases and also it controls the flow rate. The gas flow fiber loop

ringdown technique is convenient to use for several reasons, such as the large dynamic range, low cost, fast response, remotely-controllable, and chemical and electrical hazards-free.

In addition, a relative humidity sensor is an important tool for controlling and monitoring several applications. For structural health, such as for bridges, buildings, and roadways, the steel reinforcement bars is one of the essentials for concrete strength; the bars are usually inherently covered against corrosion. One of the factors that can create corrosion is chloride ions that occur inside a reinforced concrete structure. The occurrence of chlorides in the concrete usually occurs from using salt to melt snow and ice on bridges and roads through the winter seasons, especially these regions that have freezing temperature conditions [9]. Therefore, FLRD humidity sensors can be applied to monitor the humidity inside the bridges, buildings, or roadways. Another example for monitoring humidity is in fuel applications. Biomass is used to product heat and power by burning. The moisture is an important parameter that needs to be considered when biomass is utilized. The moisture often fluctuates for biomass fuels [10]. Different moisture levels give an uncertainty in the power content of the fuel that transfers to power generating a plant. Therefore, there are two ways to determine the moisture of the fuel: either by calculating the moisture and oxygen contents of the flue gases that derive from the moisture of the fuel or by straight calculation on the incoming fuel. As a result, the FLRD humidity sensor is needed in this case to monitor the humidity level.

4.3 Combining Airflow and Humidity Sensor

Newborn babies need to be monitored for the humidity of their exhaled air and also their respiratory rate [11]. In this case, monitoring humidity and respiratory rate need

a sensor with high sensitivity, small size, and fast response. Since all these requirements are available in the FLRD technique, we can apply both sensors (e.g., the humidity and the airflow sensor) to monitor the respiratory rate and humidity. These two sensors can be combined together to detect any change in the babys breath since both these sensors have different sensing mechanisms (e.g., micro-bending and evanescent field). Therefore, the FLRD (airflow/humidity) sensors can be applied inside a tracheostomy tube that is used for respiration monitoring. The sensing signal of the airflow/humidity FLRD sensor will give a fast response to any change in the respiratory rate or humidity of the infants. This sensing signal will give early warring to doctors and nurses. Figure 4.1 shows an infant respiratory device, which we can apply both sensors (e.g. airflow and humidity sensor) inside the device to monitor the humidity of the infant exhaled air and also the respiratory rate. Even in the medical field, the FLRD technique can do great work to save people's lives.

Figure 4.1 infant respiratory device

(The picture is from flometrics.com/engineering-medical-device.shtml)

4.4 References

1. Wang, C. (2009). Fiber loop ringdown—a time-domain sensing technique for multi-function fiber optic sensor platforms: current status and design perspectives. *Sensors*, 9(10), 7595-7621.

2. Wang, C. (2014). Fiber Loop Ringdown Sensors and Sensing. In Cavity-Enhanced Spectroscopy and Sensing (pp. 411-461). *Springer Berlin Heidelberg*.

3. Sahay, P., Kaya, M., and Wang, C. (2012). Fiber Loop Ringdown Sensor for Potential Real-Time Monitoring of Cracks in Concrete Structures: An Exploratory Study. *Sensors*, 13(1), 39-57.

4. Von Lerber, T. and Sigrist, M. W. (2002). Cavity-ring-down principle for fiber-optic resonators: experimental realization of bending loss and evanescent-field sensing. *Applied optics*, 41(18), 3567-3575.

5. Wang, C. and Herath, C. (2010). Fabrication and characterization of fiber loop ringdown evanescent field sensors. *Measurement Science and Technology*,21(8), 085205.

6. Wang, C., and Herath, C. (2010). High-sensitivity fiber-loop ringdown evanescent-field index sensors using single-mode fiber. *Optics letters*, 35(10), 1629-1631.

7. Belle, B. (2013). Real-time air velocity monitoring in mines-a quintessential design parameter for managing major mine health and safety hazards.*13th Coal Operators' Conference* 184-198

8. Hongqing, Z., Zeyang, S., Meiqun, Y., Zheng, L., and Jian, L. (2011). Theory Study on Nonlinear Control of Ventilation Network Airflow of Mine. *Procedia Engineering,* 26, 615-622.

9. Lam, C. C. C., Mandamparambil, R., Sun, T., Grattan, K. T., Nanukuttan, S. V., Taylor, S. E., and Basheer, P. M. (2009). Optical fiber refractive index sensor for chloride ion monitoring. *IEEE, Sensors Journal*, 9(5), 525-532.

10. Hermansson, S., Lind, F., and Thunman, H. (2011). On-line monitoring of fuel moisture-content in biomass-fired furnaces by measuring relative humidity of the flue gases. *Chemical Engineering Research and Design*, 89(11), 2470-2476.

11. Ma, Y., Ma, S., Wang, T., and Fang, W. (1995). Air-flow sensor and humidity sensor application to neonatal infant respiration monitoring. *Sensors and Actuators A: Physical*, 49(1), 47-50